NEURAL REGENERATION RESEARCH
www.nrronline.org

Research Article

Long noncoding RNA GAS5 acts as a competitive endogenous RNA to regulate GSK-3β and PTEN expression by sponging miR-23b-3p in Alzheimer's disease

Li Zeng[1, 2], Kaiyue Zhao[1, 2], Jianghong Liu[3], Mimin Liu[1, 2], Zhongdi Cai[1, 2], Ting Sun[1, 2], Zhuorong Li[1, 2, *], Rui Liu[1, 2, *]

https://doi.org/10.4103/NRR.NRR-D-23-01273
Date of submission: July 31, 2023
Date of decision: January 29, 2024
Date of acceptance: March 8, 2024
Date of web publication: July 29, 2024

From the Contents

Graphical Abstract

The regulatory mechanisms of GAS5/miR-23b-3p/GSK-3β/PTEN feedforward pathway in Alzheimer's disease

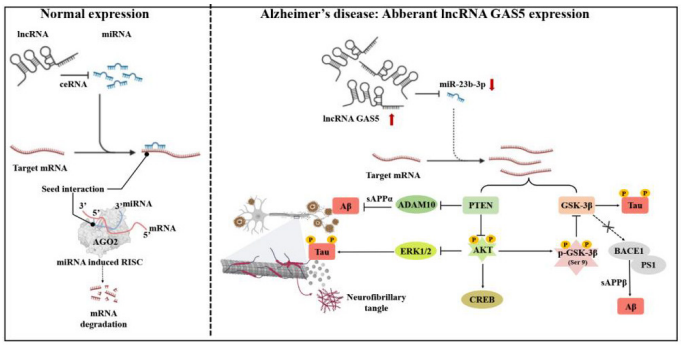

Abstract

Long noncoding RNA and microRNA are regulatory noncoding RNAs that are implicated in Alzheimer's disease, but the role of long noncoding RNA-associated competitive endogenous RNA has not been fully elucidated. The long noncoding RNA growth arrest-specific 5 (GAS5) is a member of the 5′-terminal oligopyrimidine gene family that may be involved in neurological disorders, but its role in Alzheimer's disease remains unclear. This study aimed to investigate the function of GAS5 and construct a GAS5-associated competitive endogenous RNA network comprising potential targets. RNA sequencing results showed that GAS5 was upregulated in five familial Alzheimer's disease (5×FAD) mice, APPswe/PSEN1dE9 (APP/PS1) mice, Alzheimer's disease-related APPswe cells, and serum from patients with Alzheimer's disease. Functional experiments with targeted overexpression and silencing demonstrated that GAS5 played a role in cognitive dysfunction and multiple Alzheimer's disease-associated pathologies, including tau hyperphosphorylation, amyloid-beta accumulation, and neuronal apoptosis. Mechanistic studies indicated that GAS5 acted as an endogenous sponge by competing for microRNA-23b-3p (miR-23b-3p) binding to regulate its targets glycogen synthase kinase 3beta (GSK-3β) and phosphatase and tensin homologue deleted on chromosome 10 (PTEN) expression in an Argonaute 2-induced RNA silencing complex (RISC)-dependent manner. GAS5 inhibited miR-23b-3p-mediated GSK-3β and PTEN cascades with a feedforward PTEN/protein kinase B (Akt)/GSK-3β linkage. Furthermore, recovery of GAS5/miR-23b-3p/GSK-3β/PTEN pathways relieved Alzheimer's disease-like symptoms *in vivo*, indicated by the amelioration of spatial cognition, neuronal degeneration, amyloid-beta load, and tau phosphorylation. Together, these findings suggest that GAS5 promotes Alzheimer's disease pathogenesis. This study establishes the functional convergence of the GAS5/miR-23b-3p/GSK-3β/PTEN pathway on multiple pathologies, suggesting a candidate therapeutic target in Alzheimer's disease.

Key Words: Alzheimer's disease; amyloid-beta peptide accumulation; cognitive dysfunction; competitive endogenous RNA; glycogen synthase kinase 3beta; lncRNA growth arrest-specific 5; microRNA-23b-3p; neuronal apoptosis; phosphatase and tensin homologue deleted on chromosome 10; tau phosphorylation

Introduction

Alzheimer's disease (AD) is a devastating progressive neurodegenerative disorder in the geriatric population that affects millions of people worldwide and results in a significant social burden (Masters et al., 2015). In AD patients, amyloid-beta (Aβ) deposits and neurofibrillary tangles spread throughout the brain (Nasica-Labouze et al., 2015; Li and Götz, 2017; Xing et al., 2023; Abyadeh et al., 2024). Aβ is well linked to hyperphosphorylated tau protein aggregation that coalesces to cause abnormal neuronal function and neurodegeneration (Busche and Hyman, 2020). Specific genes involved in Aβ overproduction have been identified: alpha-secretases, such as a disintegrin and metalloproteinase 10 (*ADAM10*) in the nonamyloidogenic pathway; beta-secretases, such as beta-site amyloid precursor protein cleaving enzyme 1 (*BACE1*) in the amyloidogenic pathway; gamma-secretase complex consisting of presenilins (*PS1*, *PS2*); and *NICASTRIN*. However, because the specific gene regulatory mechanisms of Aβ deposition, tau hyperphosphorylation, and neurodegeneration remain unclear, the genetic factors that influence the multiple pathological processes of AD need to be identified.

Long noncoding RNAs (lncRNAs) are characterized by a minimum length of 200

[1]Institute of Medicinal Biotechnology, Chinese Academy of Medical Sciences and Peking Union Medical College, Beijing, China; [2]State Key Laboratory of Bioactive Substances and Functions of Natural Medicines, Institute of Medicinal Biotechnology, Peking Union Medical College and Chinese Academy of Medical Sciences, Beijing, China; [3]Department of Neurology, Xuanwu Hospital, Capital Medical University, Beijing, China
***Correspondence to:** Rui Liu, PhD, liurui@imb.pumc.edu.cn; Zhuorong Li, MD, lizhuorong@imb.pumc.edu.cn.
https://orcid.org/0000-0002-8578-0733 (Rui Liu); https://orcid.org/0000-0001-5748-7444 (Zhuorong Li)

Funding: *This work was supported by the National Natural Science Foundation of China, Nos. 82173806 and U1803281; Chinese Academy of Medical Sciences (CAMS) Innovation Fund for Medical Science, Nos. 2021-I2M-1-030 and 2022-I2M-2-002; and Non-Profit Central Research Institute Fund of Chinese Academy of Medical Sciences, No. 2022-JKCS-08 (all to RL).*
How to cite this article: *Zeng L, Zhao K, Liu J, Liu M, Cai Z, Sun T, Li Z, Liu R (2026) Long noncoding RNA GAS5 acts as a competitive endogenous RNA to regulate GSK-3β and PTEN expression by sponging miR-23b-3p in Alzheimer's disease. Neural Regen Res 21(1):392-405.*

bp and having no protein-coding potential (Ruffo et al., 2023). Some lncRNAs are considered key regulators of pathological aspects of AD, including APP-cleaving enzyme 1-antisense (Fotuhi et al., 2019), nuclear enriched abundant transcript 1 (Ke et al., 2019), 51A (Ciarlo et al., 2013), and 17A (Massone et al., 2011). A regulatory mechanism named competitive endogenous RNA (ceRNA) has been recently reported to mediate lncRNA activity (Tay et al., 2014). In this interaction, lncRNA and mRNA anchor the same microRNA (miRNA) response element (MRE) and regulate the other's expression by competitively binding to the shared miRNA that blocks the target mRNA. Besides the traditional post-transcriptional regulation mechanism of lncRNAs and miRNAs, the ceRNA-based interaction provides a plausible explanation for crosstalk between different signaling branches in AD pathogenesis. However, how lncRNAs work through ceRNA in the pathological process of AD is poorly understood.

LncRNA growth arrest-specific transcript 5 (GAS5) is abundantly expressed in the cerebral cortex (Patel et al., 2023) and is involved in several biological processes, including cell proliferation, vascular remodeling, oncogenesis, and apoptosis (Wang et al., 2016; Huang et al., 2020). In AD patients, GAS5 is significantly upregulated and is correlated with hippocampal volume (Chen et al., 2022). It is involved in the pathological process of AD by regulating neuroinflammatory responses and neuronal insulin pathways (Patel et al., 2023), and suppresses axon regeneration by interacting with vimentin (Han et al., 2022). GAS5 was shown to aggravate depression-like behavior by regulating the miR-26a/early growth response gene 1 pathway (Wu et al., 2021), which indicated a role of GAS5 in neuronal injury. However, GAS5 was also reported to exert neuroprotective effects by targeting LIM homeobox 8, restoring spatial cognitive abilities in rats with cholinergic injury (Zhao et al., 2020). Given the conflicting experimental findings that GAS5 improves (Zhao et al., 2020) or impairs (Wu et al., 2021) cognitive behavior, the role and specific molecular mechanisms of GAS5 in cognition in AD remain undefined. The purpose of this study was to investigate the role and pathological mechanisms of GAS5 in AD.

Methods

Experimental animals

APPswe/PSEN1dE9 (APP/PS1), five familial AD (5×FAD) and age-matched wide-type (WT) mice were provided by the Changzhou Cavens Model Animal Co., Ltd. (Changzhou, China, license No. SCXK (Su) 2016-0010). The 6-month-old APP/PS1 mice and aged-matched WT mice (male and female in a 1:1 ratio) were specific-pathogen-free grade and weighed between 25 and 30 g. Five mice were housed per cage and were kept at 22 ± 1°C and 40% humidity, on a 12-hour light–dark cycle with free access to food and water. The *in vivo* animal research was approved and authorized by the Animal Ethics Committee of the Institute of Medicinal Biotechnology (IMB-20210419D101; approval date: April 19, 2021).

RNA sequencing assay

RNA-seq analysis was used to assess the lncRNA expression patterns of 7-month-old 5×FAD mice, 9-month-old APP/PS1 mice, and age-matched WT control mice (three mice per group, one male and two female). Total RNA from 5×FAD, APP/PS1, and WT mice was extracted with Trizol reagent (Takara, Beijing, China) and the RNA-seq platform was constructed by Sangon Biotech (Shanghai) Co., Ltd. (Shanghai, China). The lncRNA expression profile analysis was performed using a standardized RNA-seq data analysis workflow, as previously reported (Cai et al. 2022).

Adenovirus vectors and intracerebroventricular injections

Target genes loaded with recombinant adeno-associated viruses (AAVs) labeled with a green fluorescent protein were provided by Sangon Biotech, including scrambled sequences (AAV-scrambled sequences), GAS5 (AAV-GAS5), GAS5 shRNA (AAV-shGAS5), miR-23b-3p mimic (AAV-miR-23b-3p), GSK-3β shRNA (AAV-GSK-3β shRNA), and PTEN shRNA (AAV-PTEN shRNA).

The 6-month-old APP/PS1 mice were intracerebroventricularly injected with AAV-scrambled sequences, AAV-GAS5, AAV-shGAS5, AAV-GAS5+AAV-miR-23b-3p, AAV-GAS5+AAV-GSK-3β shRNA, or AAV-GAS5+AAV-PTEN shRNA. In addition, 6-month-old WT mice were intracerebroventricularly injected with AAV-scrambled sequences, AAV-GAS5, AAV-shGAS5. Each group comprised 10 mice: five male and five female. The 2.5 μL of AAV-loaded target genes were injected into the mouse lateral ventricle using a brain stereotaxic apparatus (RWD Company, Shenzhen, China). According to the mouse brain atlas (Paxinos and Franklin, 2019), the position of bregma was set to zero and the stereotaxic coordinates were as follows: medial–lateral, 1.0 mm; anterior–posterior, 1.0 mm, and dorsal–ventral, 3.0 mm.

The Morris water maze

WT and APP/PS1 mice aged 7 months were subjected to the Morris water maze (MWM) cognitive test after the AAV-loaded treatments. During the first 5 days of positioning navigation, WT and APP/PS1 mice were tasked to locate the target platform, and an electronic automatic tracking system logged the time (escape latency) and swimming speed to reach the target platform. During the probe trial on days 6 and 7, the platform was removed and the system recorded the time spent in the target area and the number of crossings at the target site to evaluate spatial memory ability of the mice.

Histochemical analysis

APP/PS1 and WT mice were anesthetized with isoflurane after the MWM test, and the brains of the mice were obtained after cardiac perfusion with normal saline and 4% paraformaldehyde. For histochemical analysis, mouse brains in each treatment group were frozen and sectioned in the coronal plane at a thickness of 25–30 μm. Thioflavin S (ThS; Sigma-Aldrich, St. Louis, MO, USA) was used to measure the β-sheet conformational characteristics of Aβ fibrils. The alkaline dye toluidine blue (Beyotime Biotech, Nanjing, China) was used for Nissl staining to assess neuronal growth status. Panoramic MIDI Digital Slice Scanner (3DHISTECH Co., Ltd., Budapest, Hungary) was used for image visualization analysis, and quantitative analysis was performed using ImageJ software version 1.52 (NIH, Bethesda, MD, USA).

Cell culture and transfection

The human Swedish APP gene was stably transfected into SH-SY5Y cells (American Type Culture Collection, Manassas, VA, USA, CRL-2266) to overproduce Aβ (termed APPswe cells). APPswe cells were treated with 300 μM copper sulfate pentahydrate (referred to as copper hereafter; BioRuler, Danbury, USA) to accelerate deposition, fibril formation, and aggregation of $A\beta_{1-42}$ due to the high binding affinity of copper with Aβ (Syme et al., 2004; Pahrudin Arrozi et al., 2017; Zeng et al., 2021; Sun et al., 2022). The miR-23b-3p mimic, miR-23b-3p inhibitor, and negative control (NC) and negative control inhibitor (NCI) were synthesized by Lainuo Biotechnology (Beijing, China). The GAS5, PTEN, and GSK-3β plasmids were obtained from OriGene (Beijing, China), and siRNAs for GAS5, PTEN, and GSK-3β were obtained from Sangon Biotech. Lipofectamine 3000 (Invitrogen, Grand Island, NY, USA) was used to transiently transfect the above plasmids to overexpress or silence the target genes. Their corresponding sequences for transfection are displayed in **Table 1**.

Table 1 | **miRNA and corresponding siRNA sequences**

Name	RNA sequence (5'–3')
GAS5 siRNA	Sense: CUU GCC UGG ACC AGC UUA AUU
	Antisense: UUA AGC UGG UCC AGG CAA GUU
Negative control	Sense: UUC UCC GAA CGU GUC ACG UTT
	Antisense: ACG UGA CAC GUU CGG AGA ATT
miR-23b-3p mimics	Sense: AUC ACA UUG CCA GGG AUU ACC AC
	Antisense: GGU AAU CCC UGG CAA UGU GAU UU
Negative control inhibitor	CAG UAC UUU UGU GUA GUA CAA
miR-23b-3p inhibitor	GUG GUA AUC CCU GGC AAU GUG AU

Cell viability assay and cell apoptosis assessment

APPswe cells were transfected with GAS5, GAS5 siRNA, and NC/NCI, and then treated with or without 300 μM copper. The viability of APPswe cells was detected by the MTT (3-(4,5-dimethylthiazol-2-yl)-2,5-diphenyltetrazolium bromide) assay (Beyotime Biotech) after the above treatments. Cell viability was calculated by measuring the absorbance at 490 nm using a multifunctional microplate photometer (Tecan Group, Menendorf, Switzerland).

Apoptosis was detected using a commercially available Annexin V-phycoerythrin (PE)/7-amino-actinomycin D (7-AAD) Apoptosis Kit (Vazyme Biotech Co., Ltd., Nanjing, China). In brief, APPswe cells in each treatment group were collected with 0.25% trypsin (without phenol red). Subsequently,

dead cells and cellular debris were removed by centrifugation at 300 × *g* for 10 minutes at 4°C (Momen-Heravi et al., 2013; Jia et al., 2022). APPswe cells were then washed twice with pre-cooled phosphate-buffered saline. The Annexin V-PE and 7-AAD staining solutions were mixed in 1:1 and then incubated for 10 minutes at 25°C in the dark. The NovoCyte flow cytometer and corresponding software (Agilent, Santa Clara, CA, USA) were used for detection and data analysis.

RNA isolation and quantitative reverse transcription-polymerase chain reaction analysis

Cytoplasmic and nuclear RNA were extracted from the cortex of 5×FAD mice using a commercial Cytoplasmic and Nuclear Purification kit (Norgen Biotek, Thorold, ON, Canada). Briefly, the cortex of 5×FAD mice was homogenized with 1% β-mercaptoethanol and centrifuged at 14,000 × g for 10 minutes. The supernatant contained cytoplasmic RNA and the pellet contained nuclear RNA. Buffer SK with 1% β-mercaptoethanol was added to both the cytoplasmic fraction and the nuclear fraction. After vortexing for 10 seconds, anhydrous ethanol was added to each mixture. Subsequently, they were transferred to a specific adsorption column and spun at 6000 × *g* for 1 minute to collect cytoplasmic and nuclear RNA.

Total RNA from APPswe cells and brain tissue was extracted and purified using Trizol reagent (Takara). Total RNA in the serum of AD patients and age-matched healthy volunteers (HAVs) was extracted using an RNA extraction kit (TIANGEN Biotech Co., Ltd., Beijing, China). Subsequently, 1 μg total RNA was reverse transcribed into complementary DNA (cDNA) using a commercially available cDNA synthesis kit (Vazyme Biotech Co., Ltd.). The cDNA template was amplified under the action of specific primers and DNA binding dye SYBY Green (Vazyme Biotech Co., Ltd.). The levels of lncRNA, mRNA or miRNA normalized to GAPDH or U6 were calculated using the $2^{-\Delta\Delta CT}$ method. The corresponding primer sequences are described in **Table 2**.

Table 2 | **Primers used for quantitative reverse transcription-polymerase chain reaction**

Gene	Primer sequence (5'–3')
GAS5	F: CTT GCC TGG ACC AGC TTA AT
	R: CAA GCC GAC TCT CCA TAC CT
GSK3B	F: GGC AGC ATG AAA GTT AGC AGA
	R: GGC GAC CAG TTC TCC TGA ATC
PTEN	F: TTG TGG TCT GCC AGC TAA AGG T
	R: GAA CTT GTC TTC CCG TCG TGT G
GAPDH	F: CAA ATT CCA TGG CAC CGT CA
	R: AGC ATC GCC CCA CTT GAT TT
Gas5	F: AGG AAT GGC AGT GTG GAC CT
	R: CCA AAT GAA CAA GCA TGC AAC C
Gsk3b	F: CCA GGA GCA GGA CAT TTC ACC
	R: CCT GAC ATC ACA CGC CAA AG
Pten	F: GCA GGA TAC GCG CTT GGG
	R: ACA GCG GCT CAA CTC TCA AA
miR-23b-3p	RT: GTC GTA TCC AGT GCA GGG TCC GAG GTA TTC GCA CTG GAT ACG ACG TGG TA
	F: CGA TCA CAT TGC CAG GGA T
	R: AGT GCA GGG TCC GAG GTA TT
U6	RT: GTC GTA TCC AGT GCA GGG TCC GAG GTA TTC GCA CTG GAT ACG ACA AAA TA
	F: CAA ATT CGT GAA GCG TTC CA
	R: AGT GCA GGG TCC GAG GTA TT

F: Forward primer; R: reverse primer. *GSK3B*, *GAS5*, and *PTEN* are human genes; *Gsk3b*, *Gas5*, and *Pten* are mouse genes.

Western blotting

Proteins were prepared from the treated APPswe cells and brain tissue of APP/PS1 mice, and expression levels were assayed by western blot analysis, as previously reported (Jiang et al., 2022; Sun et al., 2022). Briefly, the treated APPswe cells or brain tissue of APP/PS1 mice were lysed with RIPA lysis buffer composed of protease inhibitors and phosphatase inhibitors, and homogenized by tissue grinder and an ultrasonic disruptor. The lysis mixture was centrifuged at 4°C and 12,000 × *g* for 20 minutes to collect the protein supernatant. Protein concentration was detected by bicinchoninic acid assay, and protein denaturation was performed at 30 μg/20 μL at 99°C for 10 minutes. The proteins were separated via 10% sodium dodecyl sulfate–polyacrylamide gel electrophoresis at 80 V for 2 hours and then transferred to a polyvinylidene fluoride membrane at 390 mA for 70 minutes. The membranes were then incubated in 5% bovine serum albumin or milk at 25°C for 1.5 hours. The primary antibody was incubated at 4°C for 12–16 hours, and the horseradish peroxidase-labeled IgG secondary antibody was incubated at 25°C for 2 hours. The LAS4000 Fujifilm imaging system (Fujifilm, Tokyo, Japan) was used for grayscale imaging and semiquantitative analysis, for which GAPDH was used as an internal reference. The corresponding antibodies are listed in **Table 3**.

Enzyme-linked immunosorbent assay

The $A\beta_{1-40}$, $A\beta_{1-42}$, soluble APPβ (sAPPβ), and soluble APPα (sAPPα) levels were measured using specific enzyme-linked immunosorbent assay (ELISA) kits in APPswe cells (human $A\beta_{1-40}$: Cat# ml057840V, human $A\beta_{1-42}$: Cat# ml057841V, human sAPPβ: Cat# ml525880V, human sAPPα: Cat# ml025433V) and the cortex of APP/PS1 mice (mouse $A\beta_{1-40}$: Cat# ml001859V, $A\beta_{1-42}$: Cat# ml002201V, sAPPβ: Cat# ml057880V, and sAPPα: Cat# ml625251V) (all from Shanghai Enzyme-linked Biotech Co., Ltd., Shanghai, China) in accordance with the manufacturer's instructions.

Caspase-3 activity

APPswe cells were treated with GAS5, GAS5 siRNA, miR-23b-3p, miR-23b-3p+GAS5, and NC/NCI, and then caspase-3 activity was determined by a fluorescent assay kit (Abcam, Cambridge, MA, USA, Cat# ab220655). Briefly, the treated APPswe cells were lysed on ice for 10 minutes, and then 10 mM DTT 2× reaction buffer and 50 μM DEVD-AFC substrate were added to the cell lysate at 37°C for 120 minutes. The excitation wavelength was set to 400 nm, and the emission wavelength was 505 nm in the microplate reader (Tecan Group).

Dual-luciferase reporter assay

For the dual-luciferase reporter assay, 300 bp sequence fragments of GAS5, PTEN, and GSK-3β with miR-23b-3p binding sites (WT and mutant [Mut]) were ligated into the pmirGLO vector (Sangon Biotech). The Luc-WT or Luc-Mut plasmids were then co-processed with miR-23b-3p mimic or NC into HEK293 cells (American Type Culture Collection, CRL-1537). Luciferase activity and Renilla fluorescence were detected using a dual-luciferase assay kit (Vazyme Biotech Co., Ltd.). Briefly, HEK293 cells were lysed for 15 minutes at 25°C, and then centrifuged at 12,000 × *g* for 2 minutes, and the cell supernatant was collected. Next, 20 μL of cell lysis plus with 100 μL of luciferase substrate and 100 μL of Renilla working solution were added, and fluorescence was detected using a microplate reader (Tecan Group). The ratio of luciferase/Renilla was calculated as the relative fluorescence value.

RNA fluorescence *in situ* hybridization

To determine the cellular localization of GAS5 in APPswe cells, an RNA fluorescence *in situ* hybridization (FISH) detection kit and labeled probes (Gene Pharma, Shanghai, China) were used. Briefly, APPswe cells were treated with 4% paraformaldehyde for 15 minutes, perforated with 0.1% Triton-X for 15 minutes, and then blocked at 37°C for 30 minutes. Next, 1 μM SA-Cy3 and biotin-GAS5 probe working solution was denatured at 73°C for 5 minutes, and hybridized into APPswe cells overnight in the dark at 37°C. DAPI staining was performed at 25°C for 10 minutes in the dark. Image visualization analysis was performed using a confocal microscope (Zeiss, Oberkohen, Germany).

RNA-binding protein immunoprecipitation

After transfection of APPswe cells with miR-23b-3p, AGO2 siRNA, GAS5 and GAS5 siRNA, RNA immunoprecipitation was performed using a Magna RIP Immunoprecipitation Kit (Millipore, Burlington, MA, USA). Briefly, the treated APPswe cells (2×10^7/mL) were lysed with RIP lysis buffer. Subsequently, the protein lysate was incubated with A/G protein magnetic beads coupled with anti-Argonaute 2 antibody (Cell Signaling Technology, Danvers, MA, USA, Cat# 2897, RRID: AB_2096291) or anti-IgG overnight at 4°C. The protein–RNA complex was then treated with proteinase K and phenol-chloroform-isoamyl alcohol and precipitated overnight at –80°C. The precipitated RNA was purified, and the expression of GAS5, miR-23b-3p, GSK-3β, and PTEN was detected using quantitative reverse transcription-polymerase chain reaction (qRT-PCR).

Table 3 | **Primary and secondary antibodies used in western blot analysis**

Antibody	Cat#	RRID	Dilution	Supplier
Anti-tau (phospho S202 + T205, AT8) rabbit mAb	ab210703	AB_2922760	1:1000	Abcam, Cambridge, MA, USA
Anti-tau (phospho S404) rabbit mAb	ab92676	AB_10561457	1:1000	Abcam
Anti-tau (phospho S396) rabbit mAb	ab32057	AB_778254	1:1000	Abcam
Anti-tau (phospho S199) rabbit mAb	ab81268	NA	1:1000	Abcam
Anti-tau rabbit mAb	ab254256	AB_2894402	1:1000	Abcam
Anti-amyloid-beta 1–42 rabbit pAb	ab180956	NA	1:1000	Abcam
Anti-ADAM10 rabbit pAb	ab124695	AB_10972023	1:1000	Abcam
Anti-BACE1 rabbit mAb	ab183612	NA	1:1000	Abcam
Anti-PTEN (phospho S380) rabbit mAb	ab76431	AB_1524252	1:1000	Abcam
Anti-PTEN rabbit mAb	ab267787	AB_2923364	1:1000	Abcam
Anti-Akt (phospho S473) rabbit mAb	ab81283	AB_2224551	1:1000	Abcam
Anti-Akt rabbit mAb	9272	AB_329827	1:1000	CST, Danvers, MA, USA
Anti-CREB (phospho S133) rabbit mAb	ab32096	AB_731734	1:1000	Abcam
Anti-CREB rabbit mAb	ab32515	AB_2292301	1:1000	Abcam
Anti-p44/42 MAPK (ERK1/2) (phospho T202/Y204) mouse mAb	9106	AB_331768	1:1000	CST
Anti-p44/42 MAPK (ERK1/2) rabbit mAb	9102	AB_330744	1:1000	CST
Anti-GSK-3β (phospho S9) rabbit mAb	9336	AB_331405	1:1000	CST
Anti-GSK-3β rabbit mAb	9315	AB_490890	1:1000	CST
Anti-presenilin/PS1 rabbit mAb	ab76083	AB_1310605	1:1000	Abcam
Anti-amyloid precursor protein rabbit mAb	ab32136	AB_2289606	1:1000	Abcam
Anti-Bcl-2 rabbit mAb	3498	NA	1:1000	CST
Anti-Bax rabbit mAb	ab182734	NA	1:1000	Abcam
Anti-PARP rabbit mAb	9532	NA	1:1000	CST
Anti-cleaved PARP (Asp214) rabbit mAb	9541	NA	1:1000	CST
Anti-GAPDH rabbit mAb	2118	AB_561053	1:1000	CST
HRP-conjugated goat anti-rabbit IgG (H+L)	SA00001-2	AB_2722564	1:5000	Proteintech, Wuhan, Hubei, China
HRP-conjugated goat anti-mouse IgG (H+L)	SA00001-1	AB_2722565	1:5000	Proteintech

ADAM10: A disintegrin and metalloproteinase 10; APP: amyloid precursor protein; Aβ: amyloid-beta; CST: Cell Signaling Technology; GAPDH: glyceraldehyde-3-phosphate dehydrogenase; PARP: polyadenosine-diphosphate-ribose polymerase.

Human blood collection

Peripheral blood samples of 17 AD patients and 12 HAVs were collected (**Table 4**). This study was approved by the Ethics Committee of Xuanwu Hospital, Capital Medical University (approval No. linyanshen[2022]095; approval date: May 25, 2022). AD patients were diagnosed according to the National Institute of Neurological and Communicative Disorders and Stroke and the AD and Related Disorders Association (NINCDS-ADRDA) (McKhann et al., 1984; Dubois et al., 2007). All participants signed an informed consent form. The serum of blood samples was separated by centrifugation at 1000 × *g* and 4°C for 15 minutes. Total RNA was extracted from the serum and GAS5 expression was assayed using qRT-PCR as described in the section "RNA isolation and quantitative reverse transcription-polymerase chain reaction analysis."

Bioinformatic analysis

The GAS5 targets were predicted from StarBase (http://starbase.sysu.edu.cn/), DIANA-LncBase (http://www.microrna.gr/LncBase), LNCediting (http://bioinfo.life.hust.edu.cn/LNCediting/), and miRcode (http://www.mircode.org/index.php) online databases.

Statistical analysis

Unpaired *t*-tests were conducted to analyze the differences between two independent samples. One-way analysis of variance followed by Tukey's *post hoc* test was performed to analyze statistical differences between multiple groups using GraphPad Prism software, version 8.0 (GraphPad Software, San Diego, CA, USA, www.graphpad.com). Repeated measures analysis of variance followed by the least significant difference *post hoc* test was performed using SPSS software, version 25.0 (IBM, Armonk, NY, USA) to analyze the navigation test of the MWM test. The Pearson correlation coefficient was used to analyze the linear correlation between GAS5 and Mini-Mental Status examination (MMSE) scores, and between GAS5 and miR-23b-3p expression. Receiver operating characteristic (ROC) curve was used to analyze the diagnostic predominance of GAS5. $P < 0.05$ was considered statistically significant.

Results

GAS5 expression is associated with Alzheimer's disease progression

RNA expression profiles were acquired from the cortex of 7-month-old 5×FAD mice and 9-month-old APP/PS1 mice using RNA-seq. GAS5 was significantly dysregulated in the AD model mice (**Figure 1A** and **B** and **Additional Table 1**). Subsequent qRT-PCR analysis indicated increased GAS5 expression in 5×FAD ($P < 0.05$ *vs*. age-matched WT mice; **Figure 1C**) and APP/PS1 mice ($P < 0.05$ *vs*. age-matched WT mice; **Figure 1D**) compared with that in WT mice, and GAS5 was distinguishable between WT and APP/PS1 mice (area under the curve [AUC]: 0.852, $P < 0.01$; **Figure 1E**). GAS5 was also increased in copper-triggered APPswe cells at different stimulation intervals ($P < 0.05$ at 12–48 hours *vs*. 0 hours; **Figure 1F**). Evaluation of GAS5 expression in AD patients was conducted due to the possible link between GAS5 and AD. The qRT-PCR results indicated significantly high levels of GAS5 expression in the serum of AD patients compared with that of HAVs ($P < 0.01$ *vs.* HAVs; **Figure 1G**). Notably, MMSE scores were negatively correlated with GAS5 expression levels ($R^2 = 0.18$, $P < 0.05$; **Figure 1H**). ROC curve analysis indicated that GAS5 was a potential biomarker with good diagnostic value (AUC: 0.946, $P < 0.001$; **Figure 1I**). Overall, these results suggest that GAS5 dysregulation is significantly associated with the development of AD.

GAS5 silencing exerts neuroprotective effects *in vitro* and alleviates cognitive impairment *in vivo*

GAS5 overexpression and knockdown *in vitro* models were constructed by transferring pcDNA-GAS5 and GAS5 siRNA into APPswe cells (**Additional Figure 1**). GAS5 overexpression significantly decreased APPswe cell viability (both $P < 0.05$ *vs*. NC; **Figure 2A**), whereas GAS5 knockdown significantly increased it (both $P < 0.05$ *vs.* NCI; **Figure 2A**), without or with being subjected to copper. The percentages of apoptotic cells were increased after GAS5 was overexpressed in APPswe cells regardless of exposure to copper (all $P < 0.001$ *vs*. NC; **Figure 2B** and **C**), and were decreased when GAS5 was silenced (all $P < 0.05$ *vs*. NCI; **Figure 2B** and **C**), indicating that aberrant changes in GAS5 may have injury effects on neuronal cells *in vitro*. Furthermore, GAS5 upregulation

Table 4 | **Clinical data of AD patients compared to HAVs**

Variables	HAV	AD	HAV female	HAV male	AD female	AD male	*P*-value				
							AD *vs.* HAV	AD male *vs.* HAV male	AD female *vs.* HAV female	HAV male *vs.* HAV female	AD male *vs.* AD female
n	12	17	6	6	11	6					
Sex (M/F, *n*)	6/6	6/11									
Age (yr)	68.9±8.3	73.9±8.4	70.8±7.5	67.0±9.8	74.3±8.9	73.3±8.2	0.12	0.2407	0.43	0.45	0.83
MMSE	27.0±1.4	18.3±5.8	27.5±1.4	26.5±1.4	19.1±6.1	16.7±5.8	< 0.001	0.002	0.006	0.24	0.45

Data are expressed as number or mean ± SD as appropriate. AD: Alzheimer's disease; F: female; HAVs: healthy age-matched volunteers; M: male; MMSE: Mini-Mental Status Examination.

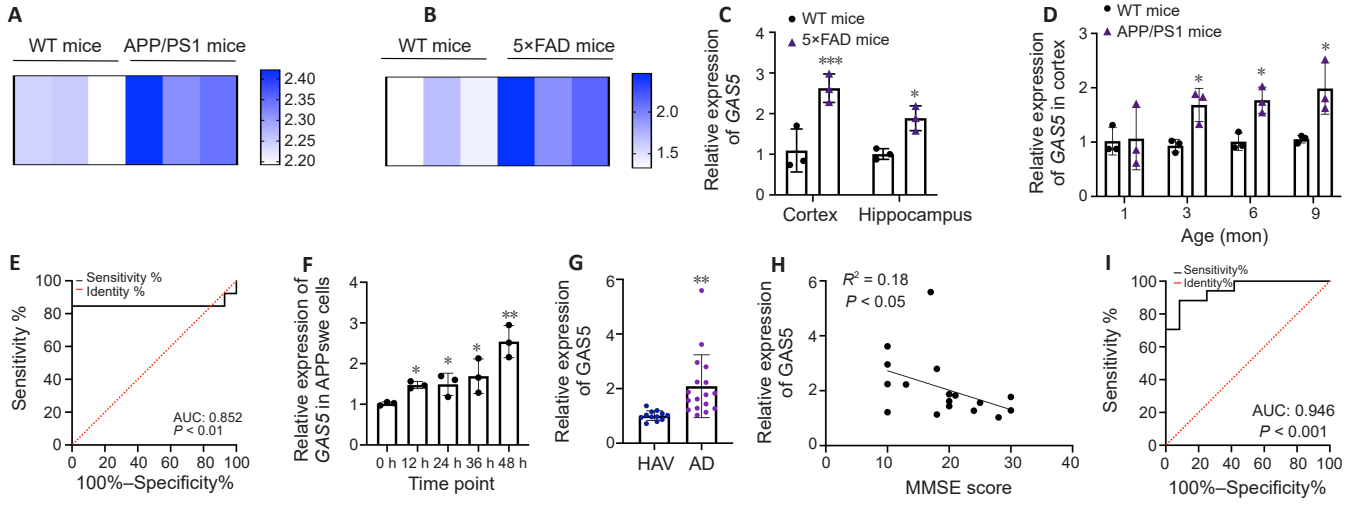

Figure 1 | **Aberrant expression of lncRNA GAS5 during AD progression.**

(A, B) GAS5 levels assessed by RNA sequencing in the cortex of 9-month-old APP/PS1 mice (A) and 7-month-old 5×FAD mice (B) compared with aged-matched WT controls (n = 3). (C) Increased expression of *GAS5* in the cortex and hippocampus of 5×FAD mice (n = 3), assessed by quantitative reverse transcription-polymerase chain reaction. (D) Increased expression of *GAS5* in the cortex of APP/PS1 mice (n = 3). (E) ROC curve for discriminating APP/PS1 mice from WT mice based on *GAS5* level. (F) Upregulated ***GAS5*** expression in APPswe cells from 0–48 hours (n = 3). (G) Increased serum GAS5 levels in AD patients (n = 17) compared with HAVs (n = 12). (H) Pearson correlation analysis of serum GAS5 levels and MMSE scores. (I) ROC curve for discriminating AD patients from HAVs in terms of serum GAS5 level (n = 12–17). Data are presented as mean ± SD. *P < 0.05, **P < 0.01, ***P < 0.001, *vs.* corresponding controls. AD: Alzheimer's disease; APP/PS1: APPswe/PSEN1dE9; AUC:area under the curve; GAS5: growth arrest-specific 5; HAVs: healthy age-matched volunteers; MMSE: Mini-Mental Status Examination; ROC: receiver operating characteristic; WT: wild-type.

decreased the ratio of antiapoptotic and apoptotic markers (Bcl-2/Bax) and increased caspase-3 activity (both P < 0.05 *vs.* NC; **Figure 2D–F**). These effects were reversed by GAS5 knockdown (both P < 0.05 *vs.* NCI; **Figure 2D–F**), suggesting that GAS5 may be involved in AD-associated injury by inducing neuronal apoptosis.

Western blot analyses showed that several phosphorylation sites of tau protein (AT8, Ser199, Ser396, and Ser404) were upregulated after GAS5 overexpression in copper-treated APPswe cells (all P < 0.05 *vs.* NC; **Figure 2D** and **E**); whereas GAS5 knockdown decreased expression of these sites (all P < 0.05 *vs.* NCI; **Figure 2D** and **E**). Additionally, GAS5 overexpression increased $A\beta_{1-42}$ levels without affecting APP levels, and decreased ADAM10 levels (both P < 0.05 *vs.* NC; **Figure 2D** and **E**), and these effects were ameliorated by silencing GAS5 (both P < 0.05 *vs.* NCI; **Figure 2D** and **E**).

To explore the biological function of GAS5 in AD *in vivo* (process diagram shown in **Additional Figure 2**), spatial cognitive behavior was evaluated using the MWM test after knockdown or overexpression of GAS5 (**Additional Figure 3**). Compared with APP/PS1 mice infused with the scrambled sequences, GAS5 knockdown APP/PS1 mice had improved learning and hippocampus-dependent memory, indicated by a shorter escape latency (P < 0.05 *vs.* APP/PS1 + scrambled control; **Figure 3A**), longer duration within the target quadrant (P < 0.05 *vs.* APP/PS1 + scrambled control; **Figure 3C**), and more platform crossings (P < 0.05 *vs.* APP/PS1 + scrambled control; **Figure 3D**). In contrast, APP/PS1 GAS5 overexpressing mice had worse cognitive impairment (all measures P < 0.05 *vs.* APP/PS1 + scrambled control; **Figure 3A**, **C** and **D**). Swimming speed did not differ between treatment groups, indicating that GAS5 knockdown and overexpression had little influence on the motor ability of mice (**Figure 3B**). Moreover, GAS5 knockdown mice had relatively precise and well-defined swimming routes, whereas GAS5 overexpression mice had chaotic and erratic routes in the probe trial performance (**Figure 3E**). Regardless of whether GAS5 was overexpressed or knocked down in WT mice, there were no detectable alterations in escape latency, number of platform crossings, or duration within the target quadrant compared with the scrambled sequences-injected WT mice (**Figure 3A**, **C** and **D**). Collectively, these results support that GAS5 plays a role in the pathophysiology of AD.

GAS5, a principal cytoplasmic lncRNA, inhibits miR-23b-3p expression by direct interaction

Before exploring GAS5 pathogenesis in AD, the distribution of GAS5 within different subcellular regions was examined. FISH experiments showed that GAS5 shuttled between the cytoplasm and nucleus in APPswe cells (**Figure 4A**), and was primarily localized in the cytoplasm in the cortex of 5×FAD mice (**Figure 4B**), indicating that GAS5 is a largely cytoplasmic lncRNA. Cytoplasmic lncRNAs have been shown to bind to miRNAs, lose their ability to interact with target mRNAs, and act as ceRNAs or sponges (Cao et al., 2018; Tang et al., 2020). Subsequent bioinformatics analyses of four databases (StarBase, miRcode, DIANA-LncBase, and LNCediting) showed GAS5 binding to four intersected miRNAs (**Figure 4C**). Of these, miR-23b-3p and miR-1297 showed better species conservation in primates and mammals (**Additional Table 2**). However, miR-1297 expression was not regulated by GAS5 overexpression or knockdown (**Additional Figure 4**). In previous studies, we identified that miR-23b-3p was dysregulated and suppressed tau phosphorylation via specific binding to GSK-3β 3′-UTR (Jiang et al., 2022). Thus, we assessed the miR-23b-3p level, which was significantly decreased when GAS5 was overexpressed (P < 0.01 *vs.* NC; **Figure 4D**), and increased when GAS5 was silenced (P < 0.01 *vs.* NCI; **Figure 4D**). The GAS5 level was significantly decreased or increased by

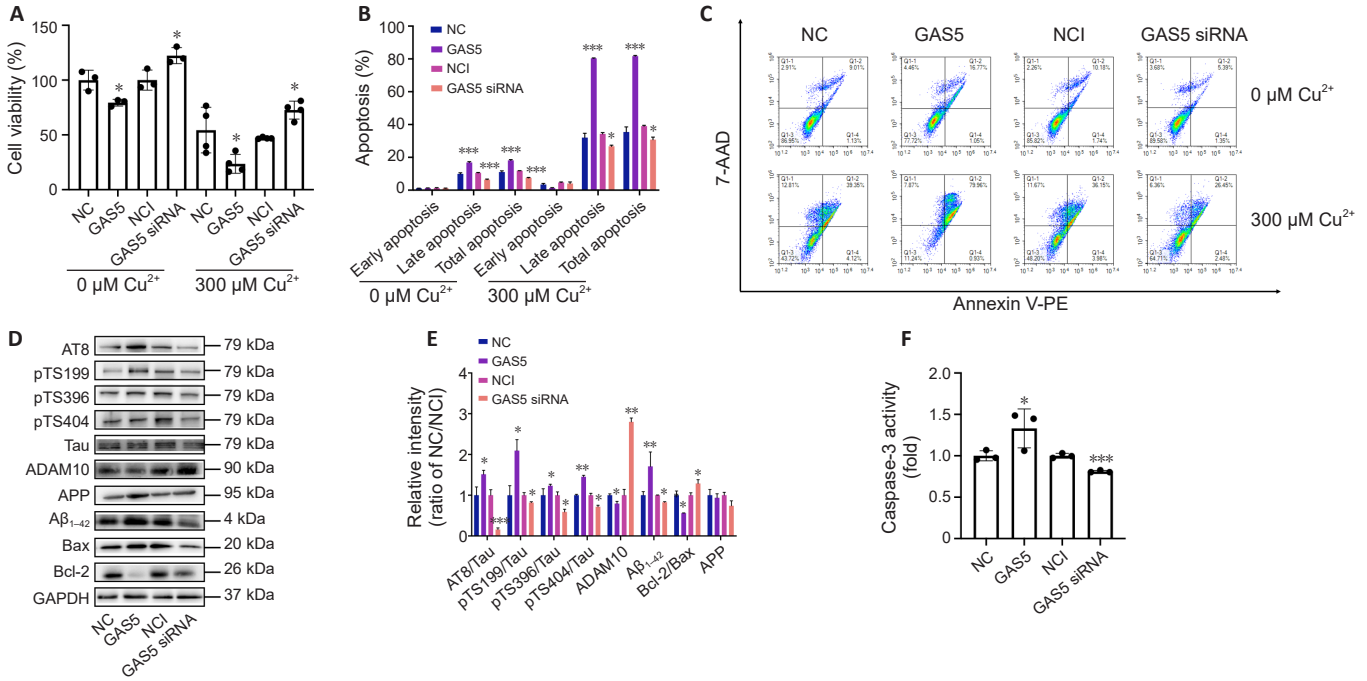

Figure 2 | **Association of GAS5 with neuronal injury, tau hyperphosphorylation, and Aβ production *in vitro*.**

(A) Cell viability of APPswe cells treated with GAS5, GAS5 siRNA, and NC and NCI treatment with (n = 4) or without (n = 3) copper for 24 hours assessed by the 3-(4,5-dimethylthiazol-2-yl)-2,5-diphenyltetrazolium bromide assay. (B, C) Percentage of apoptotic APPswe cells transfected with GAS5, GAS5 siRNA, and NC/NCI treatment with or without copper for 24 hours using flow cytometry analysis (n = 3) (B), and representative images (C). (D, E) Representative images (D) of p-Tau (Ser202 + Thr205 (AT8), Ser199, Ser396, and Ser404), Tau, ADAM10, APP, $Aβ_{1–42}$, Bax, Bcl-2 and GAPDH in copper-injured APPswe cells transfected with GAS5, GAS5 siRNA, and NC/NCI. A bar graph indicating protein quantification (n = 3) (E). (F) Caspase-3 activity in APPswe cells transfected with GAS5, GAS5 siRNA, and NC/NCI (n = 3). Data are presented as mean ± SD. *P < 0.05, **P < 0.01, ***P < 0.001, *vs.* corresponding controls (NC/NCI). ADAM10: A disintegrin and metalloproteinase 10; APP: amyloid precursor protein; Aβ: amyloid-beta; GAPDH: glyceraldehyde-3-phosphate dehydrogenase; GAS5: growth arrest-specific 5; NC: negative control; NCI: NC inhibitor.

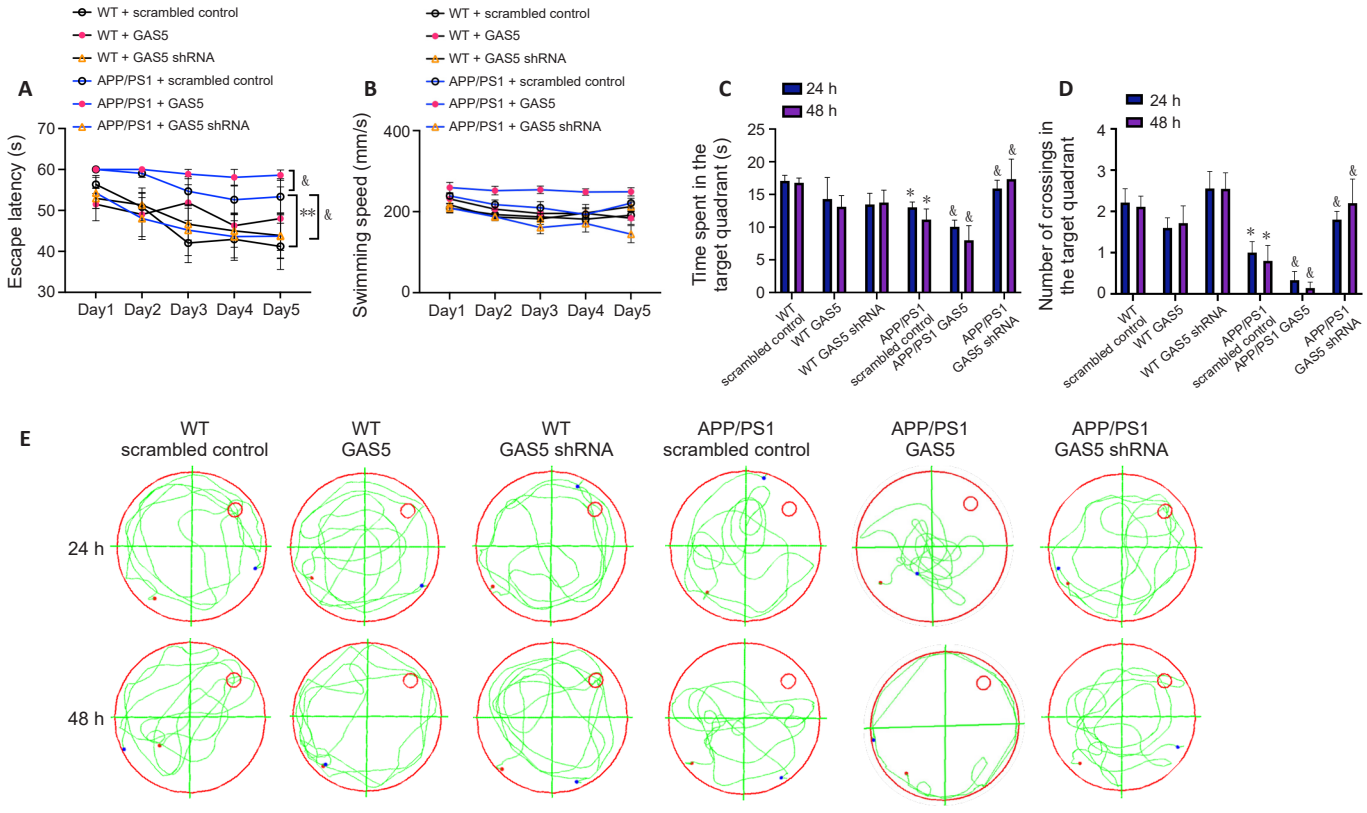

Figure 3 | **GAS5 influences cognitive dysfunction in APP/PS1 mice.**

(A) Comparison of latency in APP/PS1 and WT mice injected with AAV-GAS5, AAV-GAS5 shRNA, or scrambled sequences in the navigation test. (B) Swimming speed in each treatment group in the navigation test. (C) The time spent in the target quadrant of GAS5 or GAS5 shRNA-treated APP/PS1 mice and WT mice during probe testing. (D) Platform crossings of APP/PS1 mice and WT mice treated with AAV-GAS5, AAV-GAS5 shRNA, or scrambled sequences during probe testing. (E) Representative tracings of routes during probe testing. Data are presented as mean ± SEM, n = 10. *P < 0.05, **P < 0.01, *vs.* WT + scrambled control; &P < 0.05 *vs.* APP/PS1 + scrambled control. AAV: Adeno-associated virus; APP/PS1: APPswe/PSEN1dE9; GAS5: growth arrest-specific 5; WT: wild-type.

up- or down-regulating miR-23b-3p, respectively (both $P < 0.05$ *vs.* NC/NCI; **Figure 4E**). Furthermore, miR-23b-3p was negatively correlated with GAS5 expression in APP/PS1 mice ($R^2 = 0.605$, $P < 0.05$; **Figure 4F**).

The Starbase database indicated putative binding sites of GAS5 and miR-23b-3p (**Figure 4G**). To validate the relationship, a dual-luciferase reporter system was established using a cloning sequence of the binding site or its mutation into a luciferase vector (**Figure 4H**). miR-23b-3p inhibited luciferase activity in Luc-GAS5-Wt-transfected cells compared with cells co-transfected with NC ($P < 0.05$ *vs.* NC; **Figure 4I**). Furthermore, the GAS5 mutation sequence did not influence luciferase activity, suggesting a direct interaction of GAS5 with miR-23b-3p.

AGO2 serves as a critical regulator of miRNA silencing function, and therefore an anti-AGO2 RIP assay was performed. Endogenous GAS5 pull-down by AGO2 was significantly increased in miR-23b-3p-transfected APPswe cells ($P < 0.001$ *vs.* NC; **Figure 4J**). In contrast, AGO2 silencing attenuated AGO2-dependent degradation of GAS5 and increased the GAS5 level ($P < 0.001$ *vs.* NC; **Figure 4K**), implying that miR-23b-3p bound to GAS5 and mediated its degradation. These results support that GAS5 directly targeted miR-23b-3p and regulated its expression.

miR-23b-3p blocks the effects of GAS5 in Alzheimer's disease pathology

Given the possibility that GAS5 competes with miR-23b-3p, we explored whether miR-23b-3p would influence the effect of GAS5 in APPswe cells. The results showed that GAS5 overexpression increased apoptosis of APPswe cells (both $P < 0.001$ *vs.* NC; **Figure 5A** and **B**), and that miR-23b-3p mimic considerably reversed the pro-apoptotic function of GAS5 after copper treatment (both $P < 0.001$ *vs.* GAS5; **Figure 5A** and **B**). These results indicated that miR-23b-3p participated in the GAS5-mediated neuronal apoptotic pathway.

Next, AD-associated pathological changes in response to the interaction of GAS5 with miR-23b-3p were evaluated in APPswe cells. The levels of phosphorylated tau proteins (AT8, Ser199, Ser396, and Ser404) were significantly increased by GAS5 overexpression (all $P < 0.05$ *vs.* NC; **Figure 5C** and **D**) and reduced by miR-23b-3p mimic (all $P < 0.05$ *vs.* GAS5; **Figure 5C** and **D**). Similar to the tau protein changes, $A\beta_{1-42}$ production was increased and sAPPα was decreased by GAS5 overexpression (both $P < 0.05$ *vs.* NC; **Figure 5E** and **F**), and both were altered by miR-23b-3p mimic (both $P < 0.05$ *vs.* GAS5; **Figure 5E** and **F**). Additionally, GAS5 decreased the ADAM10 level ($P < 0.01$ *vs.* NC; **Figure 5C** and **D**) and Bcl-2/Bax ratio ($P < 0.05$ *vs.* NC; **Figure 5C** and **D**), and increased the cleaved PARP level ($P < 0.01$ *vs.* NC; **Figure 5C** and **D**) and caspase-3 activity ($P < 0.05$ *vs.* NC; **Figure 5G**), which indicated that GAS5 activated the intrinsic apoptotic pathway. Treatment with miR-23b-3p mimic showed the opposite effects (all $P < 0.05$ *vs.* GAS5; **Figure 5C**, **D**, **G**). In addition, $A\beta_{1-40}$ and sAPPβ levels involved in the amyloidogenic pathway were not significantly affected by GAS5 in the presence or absence of miR-23b-3p (**Figure 5H** and **I**). These results support that miR-23b-3p has antagonistic effects on GAS5-mediated tau hyperphosphorylation, Aβ production in the nonamyloidogenic pathway, and apoptosis, implicating an interaction between GAS5 and miR-23b-3p.

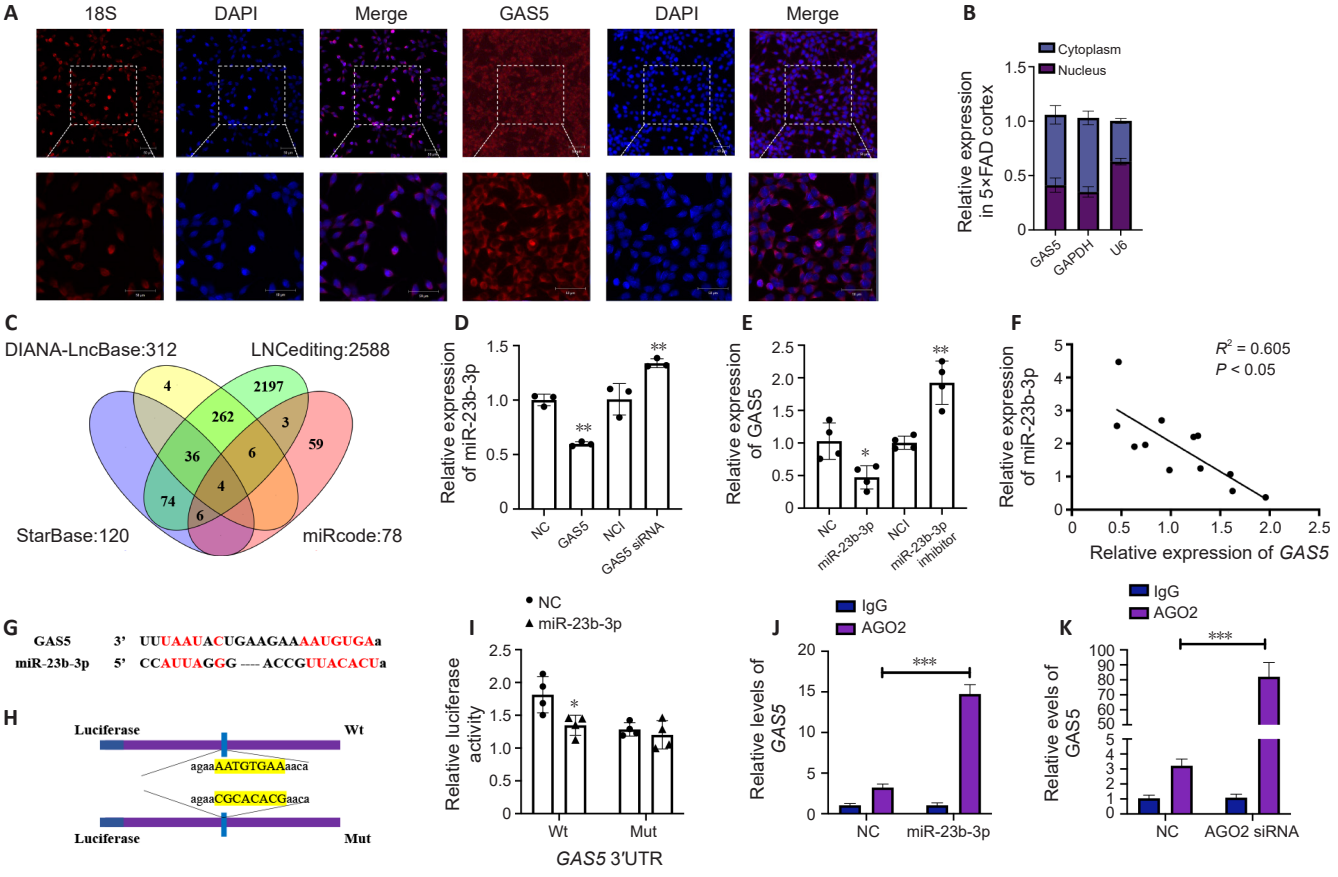

Figure 4 | **GAS5 sponges miR-23b-3p by acting as a competitive endogenous RNA.**

(A) RNA fluorescence in situ hybridization localization analysis of GAS5 (red) in APPswe cells. 18S was a positive control for cytoplasm. Scale bars: 50 μm. (B) GAS5 levels in the cytoplasm and nuclei of the cortex of 5×FAD mice ($n = 3$). GAPDH was a positive control for cytoplasm; U6 was a positive control for nuclei. (C) Bioinformatics analysis of four databases (StarBase, miRcode, DIANA-LNCBase, LNCediting). (D) Levels of miR-23b-3p in APPswe cells treated with GAS5 knockdown and GAS5 overexpression, assessed by qRT-PCR ($n = 3$). (E) GAS5 levels in APPswe cells treated with miR-23b-3p knockdown and overexpression, assessed by qRT-PCR ($n = 4$). (F) Correlation between GAS5 and miR-23b-3p in the brain of APP/PS1 mice at 1, 3, 6, and 9 months old ($n = 3$). (G) Binding site between miR-23b-3p and GAS5 using the StarBase online database. (H) Schematic representation of the wild-type (Wt) and mutant (Mut) binding sites between GAS5 and miR-23b-3p using pmirGLO vector. (I) Relative luciferase activity after co-transfection with a plasmid constructed with WT GAS5 or MUT GAS5 and NC or miR-23b-3p mimic in HEK293 cells ($n = 4$). (J) *GAS5* levels in the IgG and anti-AGO2 groups in NC or miR-23b-3p-transfected cells ($n = 3$). (K) GAS5 levels in the IgG and anti-AGO2 groups in NC or AGO2 siRNA-transfected APPswe cells ($n = 3$). Data are presented as mean ± SD. $^*P < 0.05$, $^{**}P < 0.01$, $^{***}P < 0.001$, *vs.* corresponding controls. AGO2: Argonaute RISC catalytic component 2; APP/PS1: APPswe/PSEN1dE9; DAPI: 4′,6-diamidino-2-phenylindole; GAS5: growth arrest-specific 5; NC: negative control; NCI: NC inhibitor; qRT-PCR: quantitative reverse transcription-polymerase chain reaction.

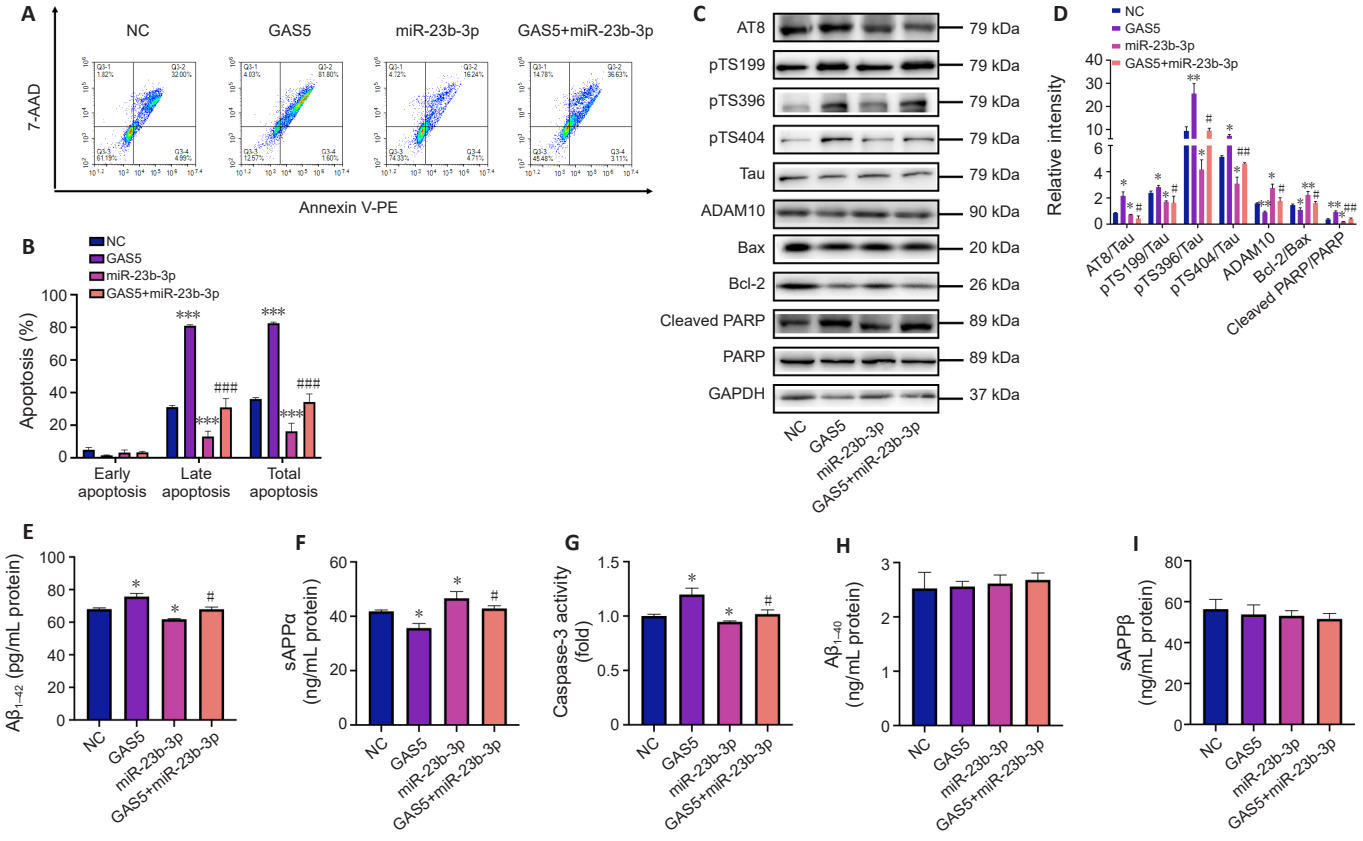

Figure 5 | **GAS5 specifically binds to miR-23b-3p during Alzheimer's disease progression.**

(A, B) Representative images (A) and quantification (B) of the effect of NC, GAS5, miR-23b-3p and GAS5+miR-23b-3p on APPswe cell apoptosis induced by 300 μM copper, assessed by flow cytometry (n = 3). (C, D) Western blots of p-Tau (AT8, Ser199, Ser396, Ser404), Tau, ADAM10, Bax, Bcl-2, cleaved PARP, PARP and GAPDH (C). A bar graph indicating protein quantification (D) in the different treatment groups of APPswe cells (n = 3). (E, F) $Aβ_{1–42}$ (E) and sAPPα (F) levels in APPswe cells of different treatment groups (n = 4). (G) Caspase-3 activity in APPswe cells of different treatment groups (n = 3). (H, I) $Aβ_{1–40}$ (H) and sAPPβ (I) levels in APPswe cells of different treatment groups (n = 4). Data are presented as mean ± SEM. *P < 0.05, **P < 0.01, ***P < 0.001, *vs.* NC; #P < 0.05, ##P < 0.01, ###P < 0.001, *vs.* GAS5. ADAM10: A disintegrin and metalloproteinase 10; Aβ: amyloid-beta; GAPDH: glyceraldehyde-3-phosphate dehydrogenase; GAS5: growth arrest-specific 5; NC: negative control; PARP: polyadenosine-diphosphate-ribose polymerase; sAPPα: soluble APPα; sAPPβ: soluble APPβ.

GAS5 acts as a ceRNA to antagonize miR-23b-3p-mediated GSK-3β and PTEN inhibition

In our previous studies, miR-23b-3p negatively regulated GSK-3β expression in AD by specifically targeting GSK-3β 3′-UTR (Jiang et al., 2022). In the present study, GSK-3β was a target of miR-23b-3p (**Additional Figure 5A–F**), and PTEN was found to be another specific target of miR-23b-3p (**Additional Figure 6A–F**) whose mRNA and protein levels were negatively regulated by miR-23b-3p (both P < 0.05 *vs.* NC; **Additional Figure 6D–F**). Follow-up analyses showed that PTEN overexpression increased apoptosis in AD cells and blocked the reduction of apoptosis by miR-23b-3p (both P < 0.001 *vs.* miR-23b-3p; **Additional Figure 6G–H**), suggesting that the miR-23b-3p/PTEN/GSK-3β pathway has a neuroprotective function in AD.

The specific crosstalk between GAS5 ansd GSK-3β/PTEN through competition for miR-23b-3p binding was further investigated. First, the potential binding sequence "UUACACU" was predicted (**Figure 6A**). Next, an AGO2-based RIP assay was used to determine whether GAS5, GSK-3β, and PTEN were enriched in the same RISC of miR-23b-3p. As expected, GAS5 overexpression (P < 0.01 *vs.* NC; **Figure 6B**) resulted in a significant decrease of GSK-3β in the AGO2 pellet (P < 0.05 *vs.* NC; **Figure 6C**), and GAS5 knockdown induced a considerable increase of PTEN pulled down by AGO2 (P < 0.05 *vs.* NC; **Figure 6D**). Of note, GAS5 bound to miR-23b-3p in an AGO2-dependent manner (**Figure 4J** and **K**). These findings support that GAS5 regulates GSK-3β and PTEN expression by sponging miR-23b-3p.

To further elucidate the role of GAS5/miR-23b-3p/GSK-3β/PTEN signaling, copper-triggered APPswe cells were treated by GAS5 knockdown or overexpression accompanied by miR-23b-3p mimic. The regulation of PTEN and GSK-3β mRNA and protein expression triggered by miR-23b-3p-occurred with the knockdown of GAS5 (all P < 0.05 *vs.* NC; **Figure 6E–H**). Moreover, miR-23b-3p overexpression markedly reversed the positive effects of GAS5 on GSK-3β and PTEN mRNA and protein levels (all P < 0.05 *vs.* GAS5; **Figure 6I–L**). Overall, these results indicate a ceRNA role of GAS5 in regulating the miR-23b-3p/GSK-3β/PTEN signaling axis in the AD model.

GAS5 induces multiple pathological processes via miR-23b-3p/GSK-3β/PTEN signaling pathways

In the experiments detailed above, GAS5 increased phosphorylated tau proteins (AT8, Ser199, Ser396, and Ser404) and $Aβ_{1–42}$ accumulation accompanied by a decrease in ADAM10, and activated the intrinsic apoptosis pathway, indicated by reduced Bcl-2/Bax ratio and increased cleaved PARP level. Next, we investigated the influence of GAS5 on the PTEN/Akt/CREB pathway, which is implicated in learning and memory processes. GAS5 upregulated PTEN and downregulated phosphorylated Akt and CREB (all P < 0.05 *vs.* NC; **Figure 7A** and **B**). miR-23b-3p reversed GAS5-mediated changes of the PTEN/Akt/CREB pathway (all P < 0.05 *vs.* GAS5; **Figure 7A** and **B**). Thus, these results support that the regulatory mechanism between GAS5 and miR-23b-3p influences multiple aspects of AD pathology, including tau hyperphosphorylation, Aβ accumulation, intrinsic apoptosis, and learning and memory impairment.

To further explore the role of GAS5 as a ceRNA, we examined the underlying molecular changes mediated by GSK-3β and PTEN after their overexpression or knockdown. GSK-3β acts as a critical kinase of tau phosphorylation (Hernandez et al., 2013). GAS5-induced upregulation of GSK-3β/p-Tau-396/p-Tau-404 signaling was blocked by miR-23b-3p mimic and GSK-3β siRNA (all P < 0.05 *vs.* GAS5; **Figure 7C** and **D**), suggesting that GAS5 regulated tau phosphorylation in a miR-23b-3p-dependent manner due to shared MREs with GSK-3β. The PI3K/Akt and ERK1/2 pathways are regulated by PTEN, which is associated with tau phosphorylation (Huang et al., 2014; Wei et al., 2019). The reduced p-Akt level and increased p-ERK1/2 level after GAS5 overexpression (both P < 0.05 *vs.* NC; **Figure 7E** and **F**), and the increased tau phosphorylation at Ser396 and Ser404 (both P < 0.05 *vs.* NC; **Figure 7E** and

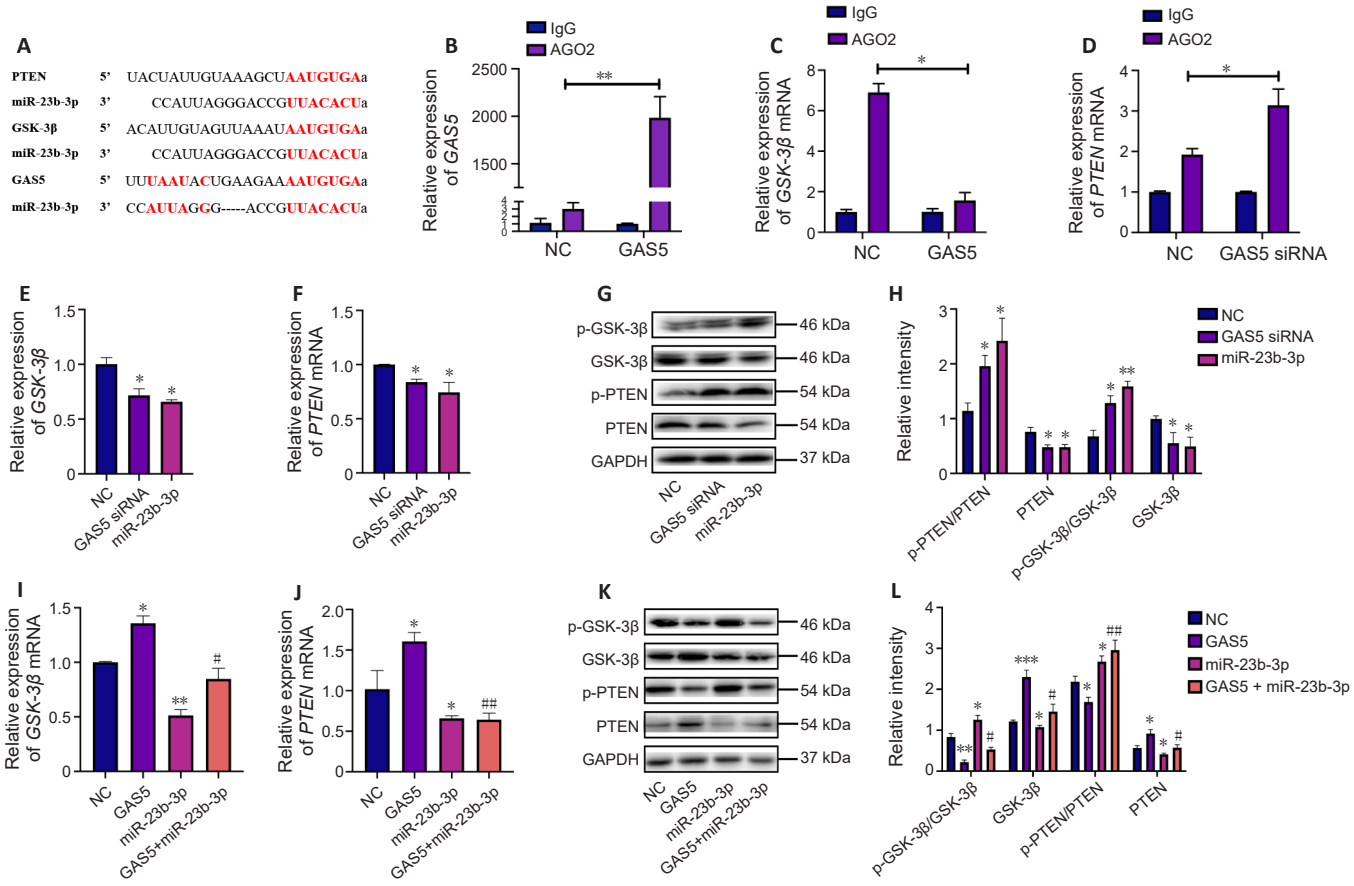

Figure 6 | **GAS5 acts as a ceRNA by sponging miR-23b-3p to upregulate GSK-3β and PTEN *in vitro*.**

(A) Putative miR-23b-3p binding sites (UUACACU) on GAS5, GSK-3β, and PTEN. (B–D) GAS5 overexpression (B) decreased GSK-3β expression (C) in the AGO2 pellet, as shown by an AGO2-based RIP assay, whereas knockdown of GAS5 increased PTEN (D) pulled down by AGO2 in APPswe cells (n = 3). (E, F) GAS5 knockdown markedly reduced the mRNA levels of *GSK-3β* (E) and *PTEN* (F), which was consistent with miR-23b-3p overexpression in APPswe cells (n = 3). (G, H) Representative images (G) and quantification (H) of p-GSK-3β, GSK-3β, p-PTEN, PTEN and GAPDH in the presence of NC, GAS5 siRNA, and miR-23b-3p in APPswe cells (n = 3). (I, J) Transcription levels of *GSK-3β* mRNA (I) and *PTEN* mRNA (J) after treatment with the NC, GAS5, miR-23b-3p, and GAS5 + miR-23b-3p in APPswe cells using quantitative reverse transcription-polymerase chain reaction analysis (n = 3). (K, L) Representative images (K) and quantification (L) of p-GSK-3β, GSK-3β, p-PTEN, PTEN and GAPDH in the presence of NC, GAS5, miR-23b-3p, and GAS5 + miR-23b-3p in APPswe cells (n = 4). Data are presented as mean ± SEM. *P < 0.05, **P < 0.01, ***P < 0.001, *vs.* NC; #P < 0.05, ##P < 0.01, *vs.* GAS5. AGO2: Argonaute RISC catalytic component 2; GAPDH: glyceraldehyde-3-phosphate dehydrogenase; GAS5: growth arrest-specific 5; GSK-3β: glycogen synthase kinase 3beta; PTEN: phosphatase and tensin homologue deleted on chromosome 10.

F), were substantially reversed by miR-23b-3p mimics and silencing of PTEN (all P < 0.05 *vs.* GAS5; **Figure 7E** and **F**), indicating that GAS5 regulates PTEN-induced tau phosphorylation via competitive binding to miR-23b-3p.

Overproduction of $A\beta_{1-42}$ was observed in response to GAS5 overexpression (P < 0.01 *vs.* NC; **Figure 7C** and **D**), but was reduced by co-transfection of GAS5 and miR-23b-3p mimic (P < 0.01 *vs.* GAS5; **Figure 7C** and **D**). Additionally, GAS5 overexpression with PTEN and GSK-3β knockdown reduced the $A\beta_{1-42}$ level (both P < 0.05 *vs.* GAS5; **Figure 7C–F**). BACE1 and PS1 levels were not affected, indicating that the amyloidogenic pathway was not involved in the GAS5/miR-23b-3p/GSK-3β signaling pathway (**Figure 7C** and **D**). However, ADAM10 expression in the nonamyloidogenic pathway was decreased by GAS5 (P < 0.05 *vs.* NC; **Figure 7E** and **F**) and restored by co-transfection of GAS5 with miR-23b-3p mimic and PTEN siRNA (both P < 0.05 *vs.* GAS5; **Figure 7E** and **F**), suggesting that GAS5-induced Aβ production has a competitive relationship with the miR-23b-3p/PTEN/ADAM10 axis.

The PI3K/Akt/GSK-3β pathway is involved in PTEN-associated tau phosphorylation (Huang et al., 2014; Chen et al., 2019), and therefore a potential association is found between these two targets of miR-23b-3p. As expected, Akt overexpression increased the levels of active p-Akt (Ser473) and inhibitory p-GSK-3β (Ser9) (both P < 0.05 *vs.* NC; **Figure 7G** and **H**), whereas Akt silencing had the opposite effects (both P < 0.05 *vs.* NCI; **Figure 7G** and **H**), which suggested a link between the GAS5/miR-23b-3p/PTEN and GAS5/miR-23b-3p/GSK-3β signaling pathways. Overall, these findings suggest that GAS5 is involved in Aβ accumulation and tau hyperphosphorylation via competition with the miR-23b-3p/PTEN/ADAM10 and miR-23b-3p/GSK-3β/PTEN pathways, within which a positive feedforward loop of PTEN/Akt/GSK-3β was established.

The GAS5/miR-23b-3p/GSK-3β/PTEN signaling pathways are involved in Alzheimer's disease *in vivo*

To elucidate the ceRNA role of GAS5 *in vivo*, the transfection efficiencies of miR-23b-3p, GSK-3β shRNA and PTEN shRNA in APP/PS1 mice were verified by qRT-PCR (**Additional Figure 7A–C**). GAS5 was overexpressed with or without miR-23b-3p, GSK-3β shRNA, and PTEN shRNA via intracerebroventricular injection with AAV vectors into APP/PS1 mice (**Additional Figure 7D**). GAS5 overexpression exacerbated cognitive impairment in APP/PS1 mice (all measures P < 0.05 ***vs.*** APP/PS1 + scrambled control; **Figure 8A**, **C**, and **D**). Notably, administration of miR-23b-3p mimic, GSK-3β shRNA, and PTEN shRNA to APP/PS1 mice significantly ameliorated the learning and hippocampus-dependent memory deficits induced by GAS5 (all measures P < 0.05 *vs.* APP/PS1 + GAS5 control; **Figure 8A**, **C**, and **D**), and these mice had more precise and well-defined travel paths in the MWM test (**Figure 8E**). Swimming speeds were indistinguishable (**Figure 8B**), indicating that the GAS5/miR-23b-3p/GSK-3β/PTEN axis had little effect on motivation. The histopathological assay results indicated that the GAS5-induced increases of Aβ deposition, characterized by Thioflavin S (ThS) staining, and neuronal loss, indicated by Nissl staining, in the APP/PS1 mice (all P < 0.05 *vs.* APP/PS1 + scrambled control; **Figure 9A–D**) were significantly reversed after co-treatment with miR-23b-3p mimic, GSK-3β shRNA, and PTEN shRNA (all P < 0.05 *vs.* APP/PS1 + GAS5 control; **Figure 9A–D**). Subsequent ELISA showed that GAS5 increased the $A\beta_{1-42}$ level and decreased the sAPPα level (both P < 0.05 *vs.* APP/PS1 + scrambled control; **Figure 9E** and **F**), and did not affect the levels of $A\beta_{1-40}$ and sAPPβ (**Figure 9G** and **H**), whereas miR-23b-3p mimic, GSK-3β shRNA, and PTEN shRNA had the opposite effects on $A\beta_{1-42}$ and sAPPα in the cortex of APP/PS1 mice (all P < 0.05 *vs.* APP/PS1 + GAS5 control; **Figure 9E** and **F**). Therefore, these results suggest a potential role of GAS5

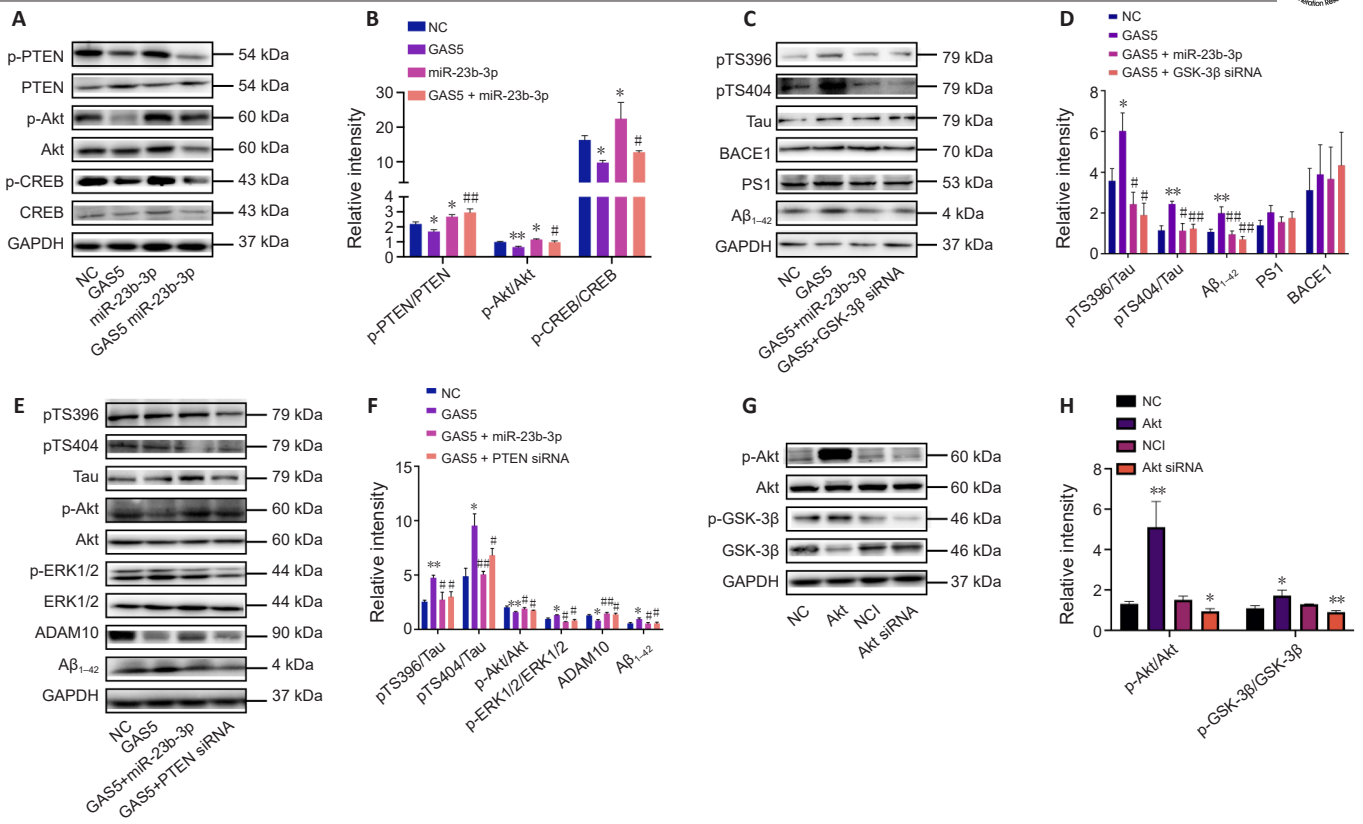

Figure 7 | **GAS5 induces tau hyperphosphorylation and Aβ production via the miR-23b-3p/GSK-3β/PTEN axis *in vitro*.**
(A, B) Representative images (A) and quantification (B) of p-PTEN, PTEN, p-Akt, Akt, p-CREB, CREB and GAPDH in APPswe cells treated with NC, GAS5, miR-23b-3p, and GAS5 + miR-23b-3p. (C, D) Representative images (C) and quantification (D) of p-Tau (Ser396 and Ser404), Tau, BACE1, PS1, $A\beta_{1-42}$, GAPDH in APPswe cells treated with NC, GAS5, GAS5 + miR-23b-3p, and GAS5 + GSK-3β siRNA. (E, F) Representative images (E) and quantification (F) of p-Tau (Ser396 and Ser404), Tau, p-Akt, Akt, p-ERK1/2, ERK1/2, ADAM10, $A\beta_{1-42}$, GAPDH in APPswe cells treated with NC, GAS5, GAS5 + miR-23b-3p, and GAS5 + PTEN siRNA. (G, H) Representative images (G) and quantification (H) of p-Akt (Ser473), Akt, p-GSK-3β (Ser 9), GSK-3β and GAPDH in APPswe cells treated with the NC/NCI, Akt, and Akt siRNA. Data are presented as mean ± SEM, $n = 3$. $^{*}P < 0.05$, $^{**}P < 0.01$, *vs.* NC/NCI; $^{\#}P < 0.05$, $^{\#\#}P < 0.01$, *vs.* GAS5. ADAM10: A disintegrin and metalloproteinase 10; AKT: protein kinase B; Aβ: amyloid-beta; BACE1: beta-site amyloid precursor protein cleaving enzyme 1; CREB: cAMP response element-binding protein; GAPDH: glyceraldehyde-3-phosphate dehydrogenase; GAS5: growth arrest-specific 5; GSK-3β: glycogen synthase kinase 3beta; PS1: presenilin-1; PTEN: phosphatase and tensin homologue deleted on chromosome 10.

in the miR-23b-3p/PTEN/GSK-3β axis involved in spatial cognition, neuronal degeneration, and amyloid load *in vivo*.

Consistent with the cognitive behavior and ceRNA action results in response to GAS5 knockdown, miR-23b-3p was upregulated and GSK-3β and PTEN were downregulated in the hippocampus of GAS5-silenced APP/PS1 mice (all $P < 0.05$ *vs.* APP/PS1 + scrambled control; **Figure 10A**). GAS5 overexpression increased tau phosphorylation (Ser396 and Ser404) and $A\beta_{1-42}$ levels in the cortex (all $P < 0.05$ *vs.* APP/PS1 + scrambled control; **Figure 10B** and **C**) and hippocampus ((all $P < 0.05$ *vs.* APP/PS1 + scrambled control; **Figure 10D** and **E**). In contrast, miR-23b-3p mimic and GSK-3β knockdown inhibited GAS5-induced increases in tau phosphorylation and $A\beta_{1-42}$ levels in the cortex (all $P < 0.05$ *vs.* APP/PS1 + GAS5 control; **Figure 10B** and **C**) and hippocampus (all $P < 0.05$ *vs.* APP/PS1 + GAS5 control; **Figure 10D** and **E**). No significant changes were observed in BACE1 and PS1 (**Figure 10B–E**), suggesting that the amyloidogenic pathway was not involved in GAS5/miR-23b-3p/GSK-3β signaling.

We next investigated the GAS5/miR-23b-3p/PTEN cascade. GAS5-induced increases in tau phosphorylation (Ser396 and Ser404) and Aβ production in the nonamyloidogenic pathway in the cortex (all $P < 0.05$ *vs.* APP/PS1 + scrambled control; **Figure 10F** and **G**) and hippocampus (all $P < 0.05$ *vs.* APP/PS1 + scrambled control; **Figure 10H** and **I**) of APP/PS1 mice were both suppressed by miR-23b-3p mimic and PTEN knockdown in the cortex (all $P < 0.05$ *vs.* APP/PS1 + GAS5 control; **Figure 10F** and **G**) and hippocampus (all $P < 0.05$ *vs.* APP/PS1 + GAS5 control; **Figure 10H** and **I**). Moreover, PTEN-induced inhibition of the Akt/ERK1/2 pathway in GAS5-overexpressing APP/PS1 mice was restored by miR-23b-3p mimic and PTEN knockdown (all $P < 0.05$ *vs.* APP/PS1 + GAS5 control; **Figure 10F–I**), which suggested the presence of feedforward regulation within the GAS5/miR-23b-3p/GSK-3β/PTEN signaling pathways. Together, these results suggest that recovery of the GAS5/miR-23b-3p/GSK-3β/PTEN pathways may help relieve AD-like symptoms *in vivo*.

Discussion

AD is a neuron-centric, unidirectional disorder initiated by Aβ deposition, which is followed by accumulation of hyperphosphorylated tau proteins into neurofibrillary tangles, ultimately leading to full-spectrum neurodegeneration with cognitive decline (Wegiel et al., 2022). Novel insights into lncRNA-based multi-targeting therapeutic strategies in AD have challenged the idea of a linearly evolving pathology and highlight the complexity of interlaced cellular pathways linked by gene regulatory networks underlying the pathogenic mechanisms (Braga et al., 2020). In this study, we found that GAS5 contributed to various aspects of AD pathology, and we propose a novel regulatory mechanism of GAS5/miR-23b-3p-targeted GSK3β/PTEN feedforward pathways.

Dysregulation of GAS5 is associated with the onset and progression of several brain disorders, including ischemic stroke (Chen et al., 2018), depression (Wu et al., 2021), and neurodegenerative diseases (Gharesouran et al., 2018; Ma et al., 2022). Although most studies report increased GAS5 expression in diseased brain, Zhao et al. (2019a) reported that GAS5 was beneficial for the recovery of PC12 cell differentiation, promotion of acetylcholine levels, and maintenance of neuronal health by regulating insulin signaling and neuroinflammation (Patel et al., 2023). The reports of correlations between GAS5 and AD are inconsistent. A previous study reported that GAS5 in peripheral blood mononuclear cells was linked to hippocampal volume in AD progression (Chen et al., 2022), whereas another study found no significant change in plasma GAS5 levels in AD patients (Khodayi et al., 2022). In the present study, RNA-seq analysis showed that GAS5 was upregulated in cognition-related brain areas of different AD models. We also established a clinical correlation between serum levels of GAS5 and cognitive ability of AD patients. We further demonstrated that GAS5 knockdown in the brain improved spatial learning and memory capabilities in APP/PS1 mice, whereas GAS5 overexpression worsened cognitive dysfunction. Additionally, GAS5

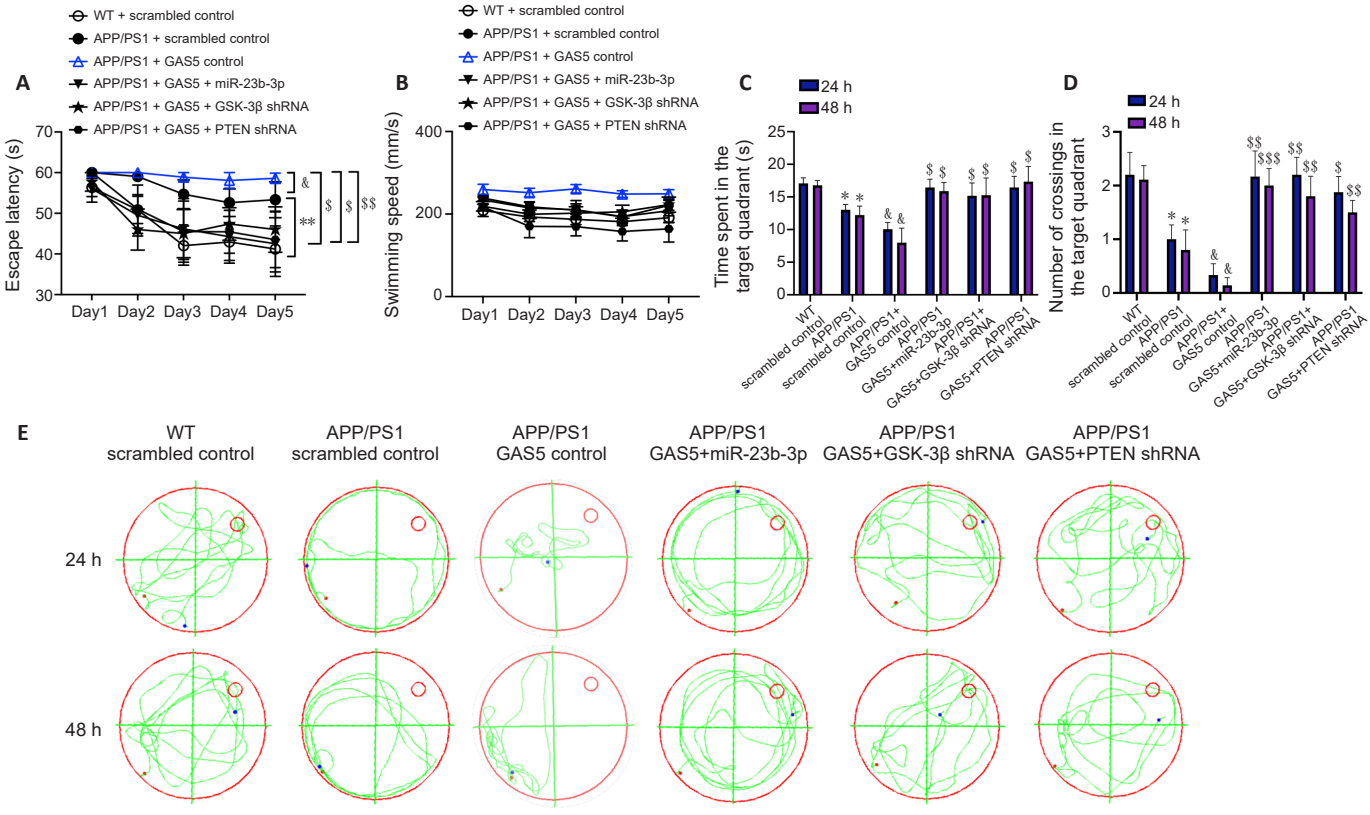

Figure 8 | **GAS5-induced cognitive deficits in Alzheimer's disease mice are rescued by miR-23b-3p overexpression, GSK-3β silencing, and PTEN silencing.**
(A) Comparison of latency in APP/PS1 mice treated with GAS5 in the presence or absence of miR-23b-3p, GSK-3β shRNA, and PTEN shRNA. (B) Swimming speed during the navigation test. (C) Duration within the target quadrant during the probe test in different treatment groups of APP/PS1 mice. (D) Platform crossings during the probe test. (E) Representative tracings of routes during the probe test. Data are presented as mean ± SEM, n = 10. *P < 0.05, **P < 0.01, *vs.* WT scrambled control; &P < 0.05, *vs.* APP/PS1 + scrambled control; \$$P$ < 0.05, \$\$$P$ < 0.01, \$\$\$$P$ < 0.001, *vs.* APP/PS1 + GAS5 controls. APP/PS1: APPswe/PSEN1dE9; GAS5: growth arrest-specific 5; GSK-3β: glycogen synthase kinase 3beta; PTEN: phosphatase and tensin homologue deleted on chromosome 10; WT: wild-type.

upregulation induced apoptosis of AD-related APPswe cells, whereas GAS5 downregulation protected these cells. Together, the findings in this study demonstrated a pathological role of GAS5 in AD, and suggest that GAS5 is a positive regulator of neuronal injury during AD progression.

Our findings showed that GAS5 participates in multiple AD-related pathological processes, namely $A\beta_{1-42}$ overproduction, tau phosphorylation, and neuronal apoptosis, eventually leading to cognitive dysfunction. Depletion of GAS5 may suppress apoptosis by correcting abnormal expression of anti-apoptotic and pro-apoptotic proteins (Zhao et al., 2019b) and facilitating cell survival via the PI3K/Akt pathway (Li et al., 2020). Another study reported that GAS5 knockdown alleviated neuroinflammatory responses and attenuated apoptosis of hippocampal neurons in a mouse model of depression (Wu et al., 2021). These reports provide evidence that GAS5 may induce degeneration in nontumorous diseases of the central nervous system, further supporting our AD-related findings.

Along with its role in neuronal apoptosis, GAS5 overexpression mediated multiple phosphorylation sites of tau protein both *in vitro* and *in vivo*, via several activated signaling pathways acting on tau phosphorylation, specifically GSK-3β, PTEN, and ERK1/2. In contrast, GAS5 knockdown decreased the expression of these phosphorylated tau sites, and inhibited the above-mentioned pathways. GAS5 also induced $A\beta_{1-42}$ overproduction and decreased sAPPα and ADAM10 levels, and these effects were ameliorated by GAS5 knockdown. sAPPα and sAPPβ are mainly generated by the cleavage of APP via the ADAM10-involved nonamyloidogenic pathway and BACE1-mediated amyloidogenic pathway (Obregon et al., 2012). Our findings indicate that GAS5 is more likely to increase $A\beta_{1-42}$ accumulation by inhibiting sAPPα production via the ADAM10-associated nonamyloidogenic pathway than by regulating the amyloidogenic signaling pathway. Moreover, we demonstrated that GAS5 upregulation led to learning and memory impairments via disruption of the Akt/CREB signaling pathway. These findings support that GAS5 plays a complex role in AD.

Considerable research has shown that an important mechanism of cytoplasmic lncRNA is the ceRNA regulatory network, which maintains and balances gene functions (Batista and Chang, 2013). As shown by the FISH and subcellular fractionation experiments, GAS5 was preferentially localized in the cytoplasm of APPswe cells. This finding is consistent with its localization in other cell types (Wei et al., 2022; Yuan et al., 2022) and indicates that GAS5 likely interacts with cytoplasmic miRNAs. Hence, online software was used to identify potential miRNAs for GAS5. miR-23b-3p is regarded as neuroprotective in various neurologic disorders (Zhan et al., 2016), including AD (Jiang et al., 2022). Interestingly, miR-23b-3p directly interacted with GAS5 in the dual-luciferase reporter gene assay (Hao et al., 2020). The subsequent qRT-PCR and RIP assays confirmed the suppressive effect of GAS5 on miR-23b-3p expression in an AGO2-dependent manner. The GAS5 overexpression-induced increases in AD-like pathology, including tau hyperphosphorylation, Aβ overproduction, and cognitive decline, were antagonized after the restoration of miR-23b-3p expression. These findings indicate that GAS5 induces AD-associated pathology via inhibiting the miR-23b-3p level.

Our previous study showed that miR-23b-3p exerted a neuroprotective effect by inhibiting tau phosphorylation through the inhibition of GSK-3β (Jiang et al., 2022). The functional convergence of miR-23b-3p's effects on AD was demonstrated by directly targeting GSK-3β and PTEN, thereby acting on tau phosphorylation, apoptosis, cognitive impairments, and even indirectly regulating Aβ processing. Our study identified the dual functional targets GSK-3β and PTEN of miR-23b-3p in AD, which are both inhibited at transcriptional and translational levels. GSK-3β is a major kinase responsible for tau phosphorylation, and its inhibitor is considered to have potential therapeutic effects for AD (Baki et al., 2004). GSK-3β activity is regulated by several upstream kinases, one of which is PTEN. PTEN negatively regulates the PI3K/Akt pathway, leading to upregulation of GSK-3β expression and activity (Feng et al., 2021). PTEN also had inhibitory effects on ADAM10 levels in a previous study (Ostalecki et al., 2017), indicating that inhibition of PTEN activity protects against neurotoxicity in AD. In the present study, the

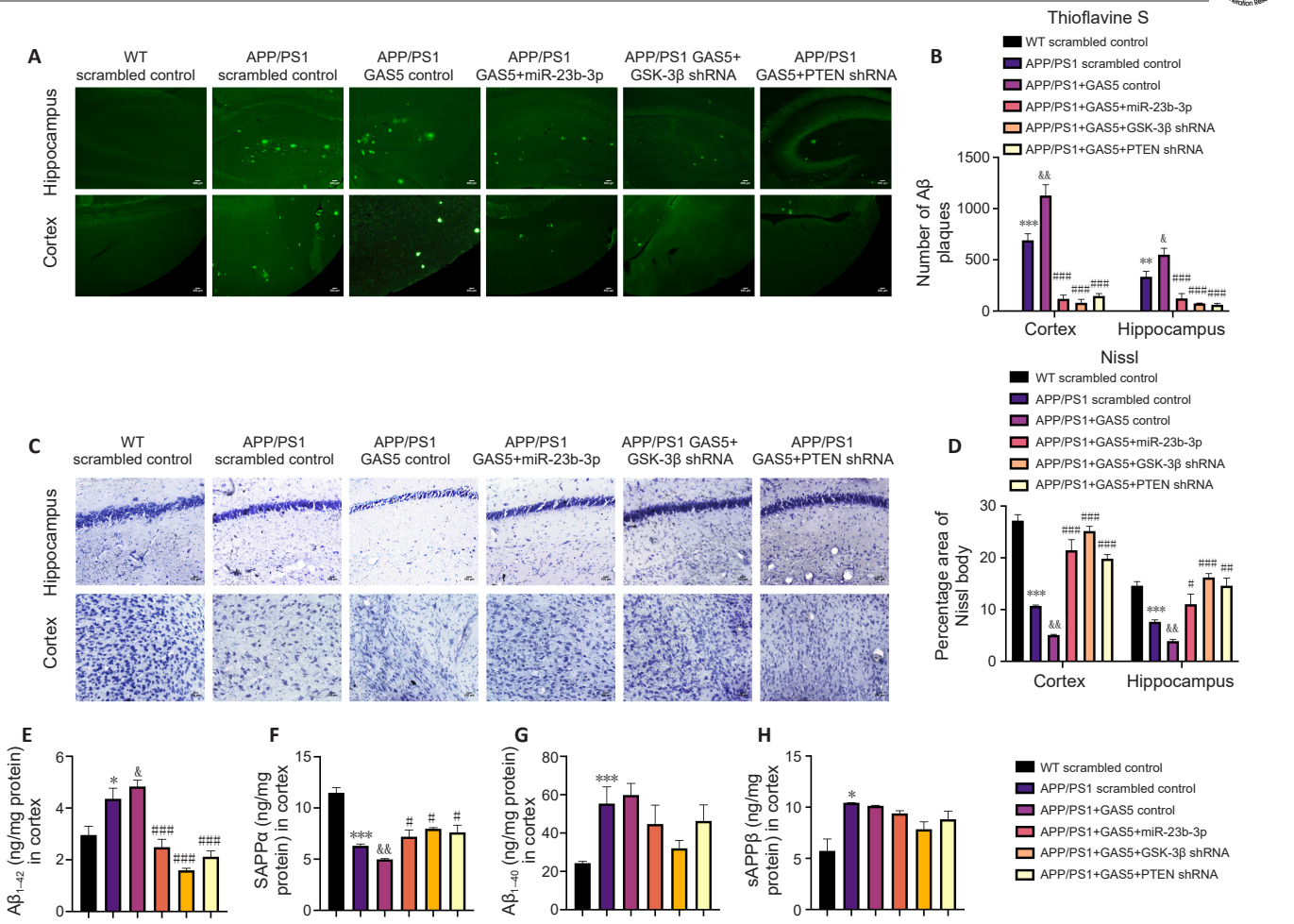

Figure 9 | **GAS5-induced Aβ aggregation and neurodegeneration in AD mice are ameliorated by miR-23b-3p overexpression, GSK-3β silencing, and PTEN silencing.**
(A, B) Representative images (A) and quantification (B) of total plaque of Thioflavin S staining in APP/PS1 mice treated with GAS5 with or without miR-23b-3p, GSK-3β shRNA, and PTEN shRNA. (C, D) Representative images (C) and quantification of Nissl staining (D) of the hippocampus and cerebral cortex of APP/PS1 mice treated with GAS5 with or without miR-23b-3p mimic, GSK-3β shRNA, and PTEN shRNA. (E–H) $A\beta_{1-42}$ (E), sAPPα (F), $A\beta_{1-40}$ (G), and sAPPβ (H) levels in the cerebral cortex of APP/PS1 mice. Data are presented as mean ± SEM, $n = 3$. *$P < 0.05$, **$P < 0.01$, ***$P < 0.001$, *vs.* WT scrambled control; &$P < 0.05$, &&$P < 0.01$, *vs.* APP/PS1 + scrambled control; #$P < 0.05$, ##$P < 0.01$, ###$P < 0.001$ *vs.* APP/PS1 + GAS5 control. APP/PS1: APPswe/PSEN1dE9; Aβ: amyloid-beta; GAS5: growth arrest-specific 5; GSK-3β: glycogen synthase kinase 3beta; PTEN: phosphatase and tensin homologue deleted on chromosome 10; sAPPα: soluble APPα; sAPPβ: soluble APPβ.

common cognate sites were explicit and a collection of GAS5, GSK-3β, and PTEN in the same RISC of miR-23b-3p was identified, suggesting that GAS5 acts as a ceRNA for the miR-23b-3p/GSK-3β/PTEN axis. In the gene gain- and loss-of-function experiments, GAS5 upregulation increased the levels of GSK-3β and PTEN, facilitated PTEN-induced Akt/ERK/p-tau and PTEN-inhibited ADAM10/Aβ pathways, and increased GSK-3β-induced tau phosphorylation. Furthermore, these effects were attenuated by miR-23b-3p overexpression and GSK-3β or PTEN knockdown.

CREB is a substrate of Akt, whose phosphatase activity is closely associated with synaptic and long-term memory (Qu et al., 2016). In the present study, the PTEN/Akt/CREB cascade was influenced by GAS5 overexpression, which is consistent with cognitive dysfunction in APP/PS1 mice. In addition, Akt phosphorylates GSK-3β at Ser9 (inactive form), and p-GSK-3β (Ser9) is decreased in the presence of Akt inhibitor (Oh et al., 2017). We found an increase in p-GSK-3β (Ser9) in response to Akt upregulation and a reversal when Akt was knocked down. Thus, a relationship between these two targets was established by the PTEN/Akt/GSK-3β (Ser9) loop, indicating a synergistic interaction of multiple cascade signals and pathological links between GAS5 and miR-23b-3p in AD.

The above results suggest that GAS5 participates in AD pathology as a ceRNA that competitively regulates the miR-23b-3p/GSK-3β/PTEN pathways. Our *in vivo* experiments further confirmed that GAS5 overexpression aggravated cognitive dysfunction in APP/PS1 mice and increased tau phosphorylation and Aβ production induced by the GSK-3β and PTEN signaling pathways. Importantly, miR-23b-3p overexpression and GSK-3β or PTEN depletion alleviated the aforementioned pathological alterations in AD mice. The regulatory mechanism of GAS5/miR-23b-3p/GSK-3β/PTEN feedforward pathways in AD is summarized in **Figure 11**.

This study had two limitations. First, the role of GAS5 in tau phosphorylation in AD needs to be explored using multiple AD models (such as 3×Tg-AD mice). Second, more comprehensive cognitive behavioral tests are required to confirm the effect of GAS5 on the miR-23b-3p/GSK-3β/PTEN pathway.

In conclusion, this study demonstrated a pathogenic function of the GAS5/miR-23b-3p/GSK-3β//PTEN axis in AD, and showed that it facilitated multiple pathologies, including cognitive deficits, tau phosphorylation, and Aβ production. The findings indicate a ceRNA mechanism underlying these actions, where GAS5 competitively binds to miR-23b-3p to activate GSK-3β and PTEN, along with a feedforward PTEN/Akt/GSK-3β linkage. Together, these findings suggest that targeting the GAS5/miR-23b-3p/GSK-3β/PTEN pathways may be a promising therapeutic approach for AD.

Author contributions: *RL and ZL conceived and directed the study. RL obtained the funding and wrote the paper. LZ, KZ, JL, ML, ZC, and TS performed the experiments and analyzed the data. All authors read and approved the final manuscript.*
Conflicts of interest: *The authors declare no conflict of interest.*
Data availability statement: *All relevant data are within the paper and its Additional files.*

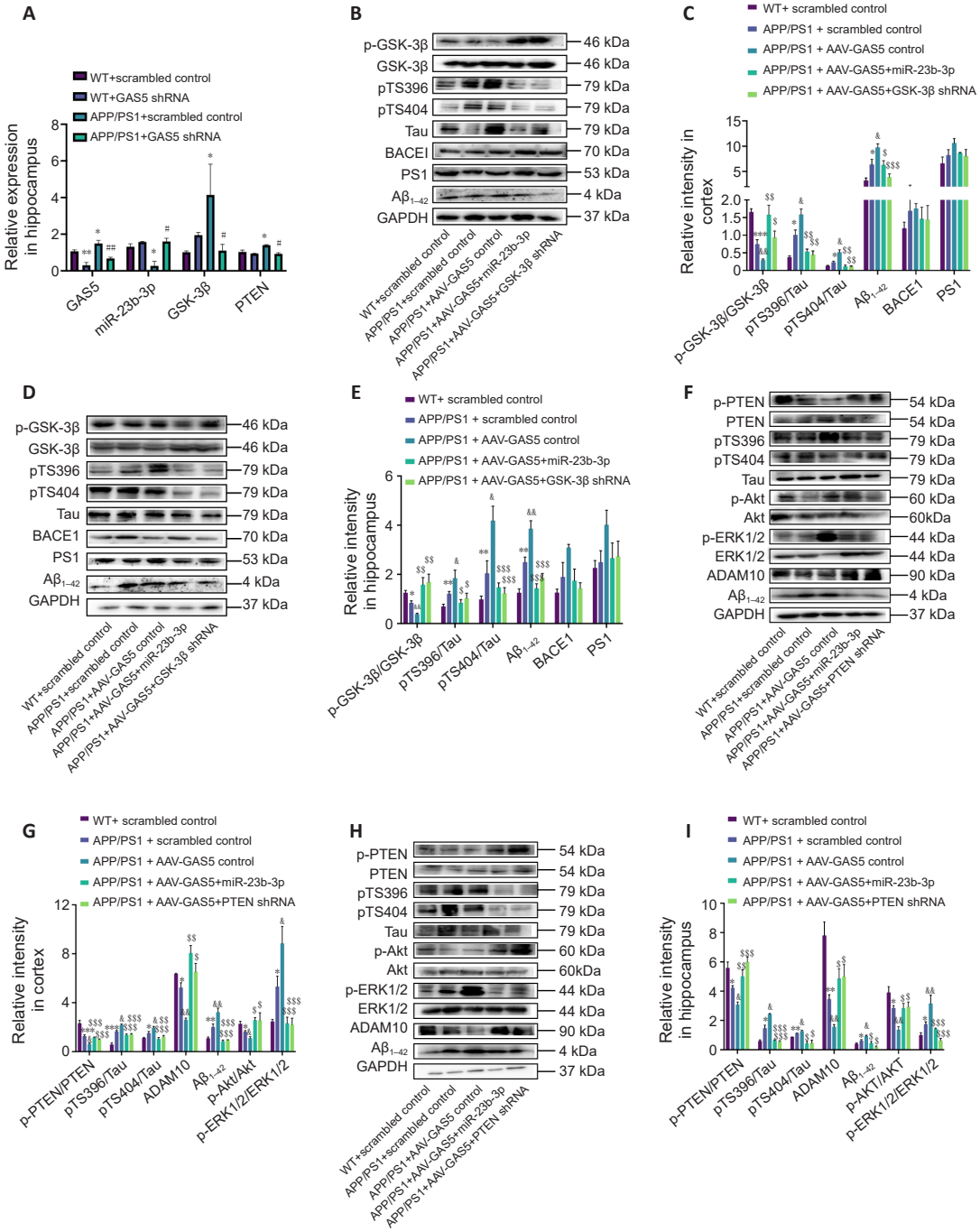

Figure 10 | GAS5 induces tau hyperphosphorylation and Aβ production via the miR-23b-3p/GSK-3β/PTEN axis in AD mice.

(A) Levels of GAS5, miR-23b-3p, GSK-3β, and PTEN assessed by qRT-PCR in WT or APP/PS1 mice injected with GAS5 shRNA or scrambled sequences. (B–E) Representative images and quantifications of p-Tau (Ser396 and Ser404), Tau, p-GSK-3β, GSK-3β, BACE1, PS1, $A\beta_{1-42}$ and GAPDH in the cortex (B, C) and hippocampus (D, E) of GAS5-treated APP/PS1 mice with or without miR-23b-3p and GSK-3β shRNA. (F–I) Representative images and quantifications of p-Tau (Ser396 and Ser404), Tau, p-PTEN, PTEN, p-ERK1/2, ERK1/2, p-Akt, Akt, ADAM10, $A\beta_{1-42}$ and GAPDH in the cortex (F, G) and hippocampus (H, I) of GAS5-treated APP/PS1 mice with or without miR-23b-3p and PTEN shRNA. Results presented as mean ± SEM, $n = 3$. $^{*}P < 0.05$, $^{**}P < 0.01$, $^{***}P < 0.001$, *vs.* WT scrambled control; $\&P < 0.05$, $\&\&P < 0.01$, *vs.* APP/PS1 + scrambled control; $\$P < 0.05$, $\$\$P < 0.01$, $\$\$\$P < 0.001$, *vs.* APP/PS1+GAS5 control. AKT: Protein kinase B; Aβ: amyloid-beta; BACE1: beta-site amyloid precursor protein cleaving enzyme 1; GAPDH: glyceraldehyde-3-phosphate dehydrogenase; GAS5: growth arrest-specific 5; GSK-3β: glycogen synthase kinase 3beta; PS1: presenilin-1; PTEN: phosphatase and tensin homologue deleted on chromosome 10; WT: wild-type.

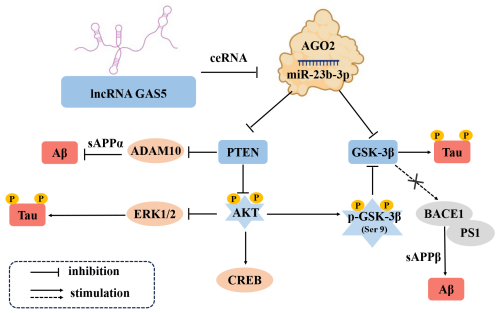

Figure 11 | Neuroprotective mechanism of GAS5/miR-23b-3p/PTEN/GSK-3B signaling proposed by the findings of this study.

GAS5 was upregulated during AD progression and regulated the miR-23b-3p/GSK-3β/PTEN-related signaling by acting as a ceRNA with a feedforward link formed by the PTEN/Akt/GSK-3β pathway. ADAM10: A disintegrin and metalloproteinase 10; Akt: protein kinase B; APP/PS1: APPswe/PSEN1dE9; Aβ: amyloid-beta; BACE1: beta-site amyloid precursor protein cleaving enzyme 1; ceRNA: competitive endogenous RNA; CREB: cAMP response element-binding protein; GAS5: growth arrest-specific 5; PS1: presenilin-1; sAPPα: soluble APPα; sAPPβ: soluble APPβ.

Additional files:

Additional Table 1: *List of aberrant lncRNA GAS5 expression from the cortex of 7-month-old 5×FAD mice and 9-month-old APP/PS1 mice using high-throughput sequencing analysis.*

Additional Table 2: *Analysis of the conservation of binding sites between growth arrest-specific 5 and four target genes.*

Additional Figure 1: *Levels of GAS5 in APPswe cells treated with GAS5 plasmid, GAS5 siRNA and NC/NCI.*

Additional Figure 2: *Flowchart of the animal experiments in this study.*

Additional Figure 3: *Levels of GAS5 in the APP/PS1 and WT mice.*

Additional Figure 4: *Unchanged miR-1297 level in APPswe cells.*

Additional Figure 5: *miR-23b-3p negatively regulates GSK-3β.*

Additional Figure 6: *miR-23b-3p negatively regulates PTEN.*

Additional Figure 7: *Levels of miR-23b-3p, GSK-3β, PTEN, and GAS5 in different treatment groups for APP/PS1 mice.*

References

Abyadeh M, Gupta V, Paulo JA, Mahmoudabad AG, Shadfar S, Mirshahvaladi S, Gupta V, Nguyen CTO, Finkelstein DI, You Y, Haynes PA, Salekdeh GH, Graham SL, Mirzaei M (2024) Amyloid-beta and tau protein beyond Alzheimer's disease. Neural Regen Res 19:1262-1276.

Baki L, Shioi J, Wen P, Shao Z, Schwarzman A, Gama-Sosa M, Neve R, Robakis NK (2004) PS1 activates PI3K thus inhibiting GSK-3 activity and tau overphosphorylation: effects of FAD mutations. EMBO J 23:2586-2596.

Batista PJ, Chang HY (2013) Long noncoding RNAs: cellular address codes in development and disease. Cell 152:1298-1307.

Braga EA, Fridman MV, Moscovtsev AA, Filippova EA, Dmitriev AA, Kushlinskii NE (2020) LncRNAs in ovarian cancer progression, metastasis, and main pathways: ceRNA and alternative mechanisms. Int J Mol Sci 21:8855.

Busche MA, Hyman BT (2020) Synergy between amyloid-β and tau in Alzheimer's disease. Nat Neurosci 23:1183-1193.

Cai Z, Zhao K, Zeng L, Liu M, Sun T, Li Z, Liu R (2022) The relationship between the aberrant long non-coding RNA-mediated competitive endogenous RNA network and Alzheimer's disease pathogenesis. Int J Mol Sci 23:8497.

Cao Z, Pan X, Yang Y, Huang Y, Shen HB (2018) The lncLocator: a subcellular localization predictor for long non-coding RNAs based on a stacked ensemble classifier. Bioinformatics 34:2185-2194.

Chen F, Zhang L, Wang E, Zhang C, Li X (2018) LncRNA GAS5 regulates ischemic stroke as a competing endogenous RNA for miR-137 to regulate the Notch1 signaling pathway. Biochem Biophys Res Commun 496:184-190.

Chen X, Ren G, Li Y, Chao W, Chen S, Li X, Xue S (2022) Level of LncRNA GAS5 and hippocampal volume are associated with the progression of Alzheimer's disease. Clin Interv Aging 17:745-753.

Chen YX, Zhu DY, Gao J, Xu ZL, Tao SC, Yin WJ, Zhang YL, Gao YS, Zhang CQ (2019) Diminished membrane recruitment of Akt is instrumental in alcohol-associated osteopenia via the PTEN/Akt/GSK-3β/β-catenin axis. FEBS J 286:1101-1119.

Ciarlo E, Massone S, Penna I, Nizzari M, Gigoni A, Dieci G, Russo C, Florio T, Cancedda R, Pagano A (2013) An intronic ncRNA-dependent regulation of SORL1 expression affecting Aβ formation is upregulated in post-mortem Alzheimer's disease brain samples. Dis Model Mech 6:424-433.

Dubois B, Feldman HH, Jacova C, Dekosky ST, Barberger-Gateau P, Cummings J, Delacourte A, Galasko D, Gauthier S, Jicha G, Meguro K, O'brien J, Pasquier F, Robert P, Rossor M, Salloway S, Stern Y, Visser PJ, Scheltens P (2007) Research criteria for the diagnosis of Alzheimer's disease: revising the NINCDS-ADRDA criteria. Lancet Neurol 6:734-746.

Feng C, Chen Y, Zhang Y, Yan Y, Yang M, Gui H, Wang M (2021) PTEN regulates mitochondrial biogenesis via the AKT/GSK-3β/PGC-1α pathway in autism. Neuroscience 465:85-94.

Fotuhi SN, Khalaj-Kondori M, Hoseinpour Feizi M A, Talebi M (2019) Long non-coding RNA BACE1-AS may serve as an Alzheimer's disease blood-based biomarker. J Mol Neurosci 69:351-359.

Gharesouran J, Taheri M, Sayad A, Ghafouri-Fard S, Mazdeh M, Omrani MD (2018) The growth arrest-specific transcript 5 (GAS5) and nuclear receptor subfamily 3 group c member 1 (NR3C1): novel markers involved in multiple sclerosis. Int J Mol Cell Med 7:102-110.

Han X, Xu J, Chen Z, Li P, Zhao L, Tao J, Shen Y, Zhu S, Yu B, Zhu J, Cao Q, Zhou S (2022) Gas5 inhibition promotes the axon regeneration in the adult mammalian nervous system. Exp Neurol 356:114157.

Hao X, Li H, Zhang P, Yu X, Jiang J, Chen S (2020) Down-regulation of lncRNA Gas5 promotes hypoxia-induced pulmonary arterial smooth muscle cell proliferation by regulating KCNK3 expression. Eur J Pharmacol 889:173618.

Hernandez F, Lucas JJ, Avila J (2013) GSK3 and tau: two convergence points in Alzheimer's disease. J Alzheimers Dis 33 Suppl 1:S141-144.

Huang H, Tang D, Xu K, Jiang Z (2014) Curcumin attenuates amyloid-β-induced tau hyperphosphorylation in human neuroblastoma SH-SY5Y cells involving PTEN/Akt/GSK-3β signaling pathway. J Recept Signal Transduct Res 34:26-37.

Huang W, Shi Y, Han B, Wang Q, Zhang B, Qi C, Liu F (2020) LncRNA GAS5-AS1 inhibits glioma proliferation, migration, and invasion via miR-106b-5p/TUSC2 axis. Hum Cell 33:416-426.

Jia Y, Yu L, Ma T, Xu W, Qian H, Sun Y, Shi H (2022) Small extracellular vesicles isolation and separation: Current techniques, pending questions and clinical applications. Theranostics 12:6548-6575.

Jiang H, Liu J, Guo S, Zeng L, Cai Z, Zhang J, Wang L, Li Z, Liu R (2022) miR-23b-3p rescues cognition in Alzheimer's disease by reducing tau phosphorylation and apoptosis via GSK-3β signaling pathways. Mol Ther Nucleic Acids 28:539-557.

Ke S, Yang Z, Yang F, Wang X, Tan J, Liao B (2019) Long noncoding RNA NEAT1 aggravates Aβ-induced neuronal damage by targeting miR-107 in Alzheimer's disease. Yonsei Med J 60:640-650.

Khodayi M, Khalaj-Kondori M, Hoseinpour Feizi MA, Jabarpour Bonyadi M, Talebi M (2022) Plasma lncRNA profiling identified BC200 and NEAT1 lncRNAs as potential blood-based biomarkers for late-onset Alzheimer's disease. EXCLI J 21:772-785.

Li C, Götz J (2017) Tau-based therapies in neurodegeneration: opportunities. and challenges. Nat Rev Drug Discov 16:863-883.

Li J, Lv H, Che YQ (2020) Long non-coding RNA Gas5 potentiates the. effects of microRNA-21 downregulation in response to ischaemic brain injury. Neuroscience 437:87-97.

Ma J, Sun W, Chen S, Wang Z, Zheng J, Shi X, Li M, Li D, Gu Q (2022) The long noncoding RNA GAS5 potentiates neuronal injury in Parkinson's disease by binding to microRNA-150 to regulate Fosl1 expression. Exp Neurol 347:113904.

Massone S, Vassallo I, Fiorino G, Castelnuovo M, Barbieri F, Borghi R, Tabaton M, Robello M, Gatta E, Russo C, Florio T, Dieci G, Cancedda R, Pagano A (2011) 17A, a novel non-coding RNA, regulates GABA B alternative splicing and signaling in response to inflammatory stimuli and in Alzheimer disease. Neurobiol Dis 41:308-317.

Masters CL, Bateman R, Blennow K, Rowe CC, Sperling RA, Cummings JL (2015) Alzheimer's disease. Nat Rev Dis Primers 1:15056.

McKhann G, Drachman D, Folstein M, Katzman R, Price D, Stadlan EM (1984) Clinical diagnosis of Alzheimer's disease: report of the NINCDS-ADRDA Work Group under the auspices of Department of Health and Human Services Task Force on Alzheimer's Disease. Neurology 34:939-944.

Momen-Heravi F, Balaj L, Alian S, Mantel PY, Halleck AE, Trachtenberg AJ, Soria CE, Oquin S, Bonebreak CM, Saracoglu E, Skog J, Kuo WP (2013) Current methods for the isolation of extracellular vesicles. Biol Chem 394:1253-1262.

Nasica-Labouze J, et al. (2015) Amyloid β protein and Alzheimer's disease: when computer simulations complement experimental studies. Chem Rev 115:3518-3563.

Obregon D, Hou H, Deng J, Giunta B, Tian J, Darlington D, Shahaduzzaman M, Zhu Y, Mori T, Mattson MP, Tan J (2012) Soluble amyloid precursor protein-α modulates β-secretase activity and amyloid-β generation. Nat Commun 3:777.

Oh S, Kim H, Nam K, Shin I (2017) Silencing of Glut1 induces chemoresistance via modulation of Akt/GSK-3β/β-catenin/survivin signaling pathway in breast cancer cells. Arch Biochem Biophys 636:110-122.

Ostalecki C, Lee JH, Dindorf J, Collenburg L, Schierer S, Simon B, Schliep S, Kremmer E, Schuler G, Baur AS (2017) Multiepitope tissue analysis reveals SPPL3-mediated ADAM10 activation as a key step in the transformation of melanocytes. Sci Signal 10:eaai8288.

Pahrudin Arrozi A, Shukri SNS, Wan Ngah WZ, Mohd Yusof YA, Ahmad Damanhuri MH, Makpol S (2017) Evaluation of the expression of amyloid precursor protein and the ratio of secreted amyloid beta 42 to amyloid beta 40 in SH-SY5Y cells stably transfected with wild-type, single-mutant and double-mutant forms of the APP gene for the study of Alzheimer's disease pathology. Appl Biochem Biotechnol 183:853-866.

Patel RS, Lui A, Hudson C, Moss L, Sparks RP, Hill SE, Shi Y, Cai J, Blair LJ, Bickford PC, Patel NA (2023) Small molecule targeting long noncoding RNA GAS5 administered intranasally improves neuronal insulin signaling and decreases neuroinflammation in an aged mouse model. Sci Rep 13:317.

Paxinos G, Franklin KBJ (2019) Paxinos and Franklin's the mouse brain in stereotaxic coordinates. 5th ed. Boston: Elsevier/Academic Press.

Qu L, Gao Y, Sun H, Wang H, Liu X, Sun D (2016) Role of PTEN-Akt-CREB signaling pathway in nervous system impairment of rats with chronic arsenite exposure. Biol Trace Elem Res 170:366-372.

Ruffo P, De Amicis F, Giardina E, Conforti FL (2023) Long-noncoding RNAs as epigenetic regulators in neurodegenerative diseases. Neural Regen Res 18:1243-1248.

Sun T, Zhao K, Liu M, Cai Z, Zeng L, Zhang J, Li Z, Liu R (2022) miR-30a-5p induces Aβ production via inhibiting the nonamyloidogenic pathway in Alzheimer's disease. Pharmacol Res 178:106153.

Syme C, Nadal R, Rigby S, Viles J (2004) Copper binding to the amyloid-beta (Abeta) peptide associated with Alzheimer's disease: folding, coordination geometry, pH dependence, stoichiometry, and affinity of Abeta-(1-28): insights from a range of complementary spectroscopic techniques. J Biol Chem 279:18169-18177.

Tang H, Han X, Feng Y, Hao Y (2020) linc00968 inhibits the tumorigenesis and metastasis of lung adenocarcinoma via serving as a ceRNA against miR-9-5p and increasing CPEB3. Aging (Albany NY) 12:22582-2259.

Tay Y, Rinn J, Pandolfi PP (2014) The multilayered complexity of ceRNA crosstalk and competition. Nature 505:344-352.

Wang Y, Shan K, Yao M, Yao J, Wang J, Li X, Liu B, Zhang Y, Ji Y, Jiang Q, Yan B (2016) Long noncoding RNA-GAS5: a novel regulator of hypertension-induced vascular remodeling. Hypertension 68:736-748.

Wegiel J, et al. (2022) Developmental deficits and staging of dynamics of age associated Alzheimer's disease neurodegeneration and neuronal loss in subjects with Down syndrome. Acta Neuropathol Commun 10:2.

Wei J, Zeng Y, Yang Q, Ke H, Fu G, Zheng Y, Lu J (2022) GAS5 suppresses cell proliferation, migration, and invasion via the miR-455-5p/CDKN1B axis in cutaneous squamous cell carcinoma. Crit Rev Eukaryot Gene Expr 32:63-76.

Wei Z, Mahaman Y, Zhu F, Wu M, Xia Y, Zeng K, Yang Y, Liu R, Wang JZ, Shu X, Wang X (2019) GSK-3β and ERK1/2 incongruously act in tau hyperphosphorylation in SPS-induced PTSD rats. Aging (Albany NY) 11:7978-7995.

Wu Y, Rong W, Jiang Q, Wang R, Huang H (2021) Downregulation of lncRNA GAS5 alleviates hippocampal neuronal damage in mice with depression-like behaviors via modulation of microRNA-26a/EGR1 axis. J Stroke Cerebrovasc Dis 30:105550.

Xing ZK, Du LS, Fang X, Liang H, Zhang SN, Shi L, Kuang CX, Han TX, Yang Q (2023) The relationship among amyloid-β deposition, sphingomyelin level, and the expression and function of P-glycoprotein in Alzheimer's disease pathological process. Neural Regen Res 18:1300-1307.

Yuan X, Jing Y, Guang M, Zhu J, Wang J, Wang Y, Zhang Y (2022) GAS5 alleviates cisplatin drug resistance in oral squamous cell carcinoma by sponging miR-196a. J Int Med Res 50:3000605221132456.

Zeng L, Jiang H, Ashraf GM, Liu J, Wang L, Zhao K, Liu M, Li Z, Liu R (2021) Implications of miR-148a-3p/p35/PTEN signaling in tau hyperphosphorylation and autoregulatory feedforward of Akt/CREB in Alzheimer's disease. Mol Ther Nucleic Acids 27:256-275.

Zhan L, Yao Y, Fu H, Li Z, Wang F, Zhang X, He W, Zheng W, Zhang Y, Zheng H (2016) Protective role of miR-23b-3p in kainic acid-induced seizure. Neuroreport 27:764-768.

Zhao H, Jin T, Cheng X, Qin J, Zhang L, He H, Xue J, Jin G (2020) GAS5 which is regulated by Lhx8 promotes the recovery of learning and memory in rats with cholinergic nerve injury. Life Sci 260:118388.

Zhao HY, Zhang ST, Cheng X, Li HM, Zhang L, He H, Qin JB, Zhang WY, Sun Y, Jin GH (2019a) Long non-coding RNA GAS5 promotes PC12 cells differentiation into Tuj1-positive neuron-like cells and induces cell cycle arrest. Neural Regen Res 14:2118-2125.

Zhao JH, Wang B, Wang XH, Xu CW (2019b) Effect of lncRNA GAS5 on the apoptosis of neurons via the notch1 signaling pathway in rats with cerebral infarction. Eur Rev Med Pharmacol Sci 23:10083-10091.

C-Editor: Zhao M; S-Editor: Li CH; L-Editors: Li CH, Song LP; T-Editor: Jia Y

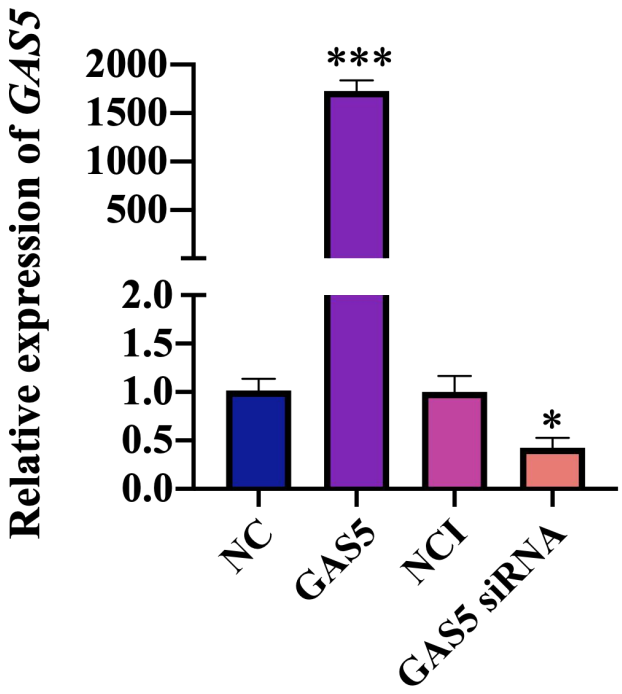

Additional Figure 1 Levels of GAS5 in APPswe cells treated with GAS5, GAS5 siRNA and NC/NCI.
Data are presented as mean ± SEM, $n = 3$. $^{*}P < 0.05$, $^{***}P < 0.001$, *vs*. NC/NCI. GAS5: Growth arrest-specific 5; NC: negative control; NCI: negative control inhibitor.

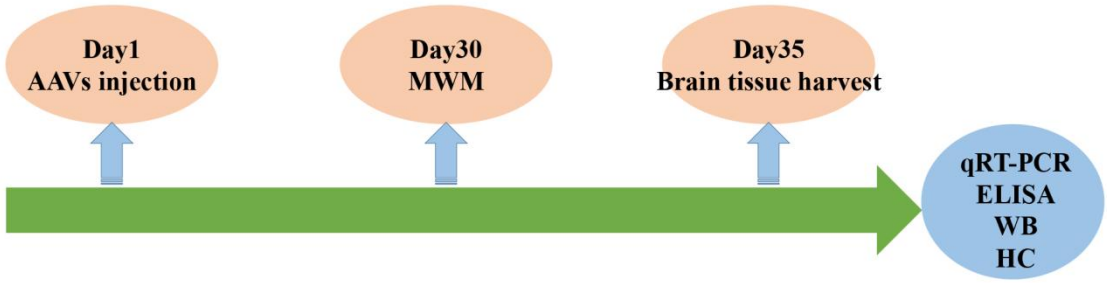

Additional Figure 2 Flowchart of the animal experiments in this study.

AAVs: Adeno-associated viruses; ELISA: Enzyme-linked immunosorbent assay; HC: Histochemical analysis; MWM: Morris water maze; qRT-PCR: quantitative reverse transcription-polymerase chain reaction; WB: western blotting.

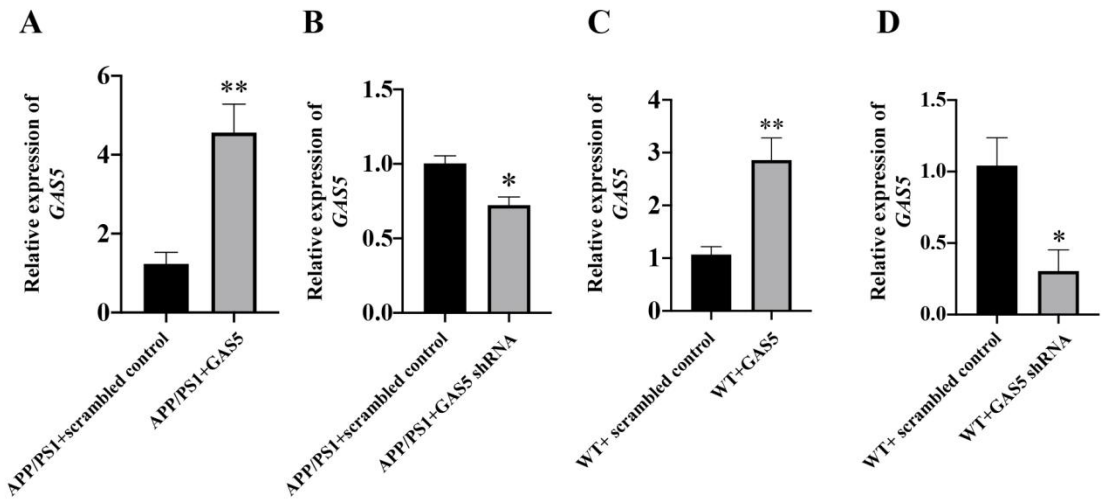

Additional Figure 3 Levels of GAS5 in the APP/PS1 and WT mice.

Increased GAS5 levels in the hippocampus of APP/PS1 mice (A) and WT mice (C) after intracerebroventricular injection of AAVs-scrambled sequences, AAVs-GAS5. Decreased levels of GAS5 in the hippocampus of APP/PS1 mice (B) and WT mice (D) after intracerebroventricular injection of AAVs-scrambled sequences and AAVs-GAS5 shRNA. Data are presented as mean ± SEM, $n = 3$. $^{*}P < 0.05$, $^{**}P < 0.01$, *vs.* APP/PS1+ scrambled controls or WT+ scrambled controls. AAVs: Adeno-associated virus; APP/PS1: APPswe/PSEN1dE9; GAS5: growth arrest-specific 5; WT: wild-type.

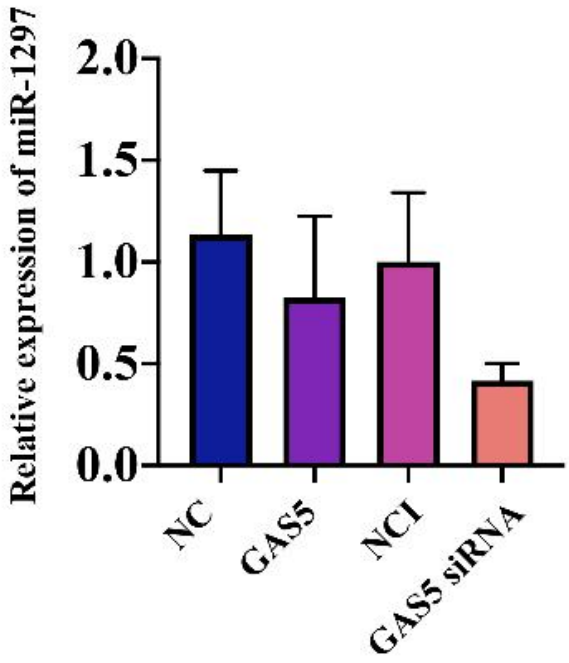

Additional Figure 4 Unchanged miR-1297 level in APPswe cells treated with GAS5, GAS5 siRNA and NC/NCI.
Data are presented as mean ± SEM, *n* = 3. GAS5: Growth arrest-specific 5; NC: negative control; NCI: negative control inhibitor.

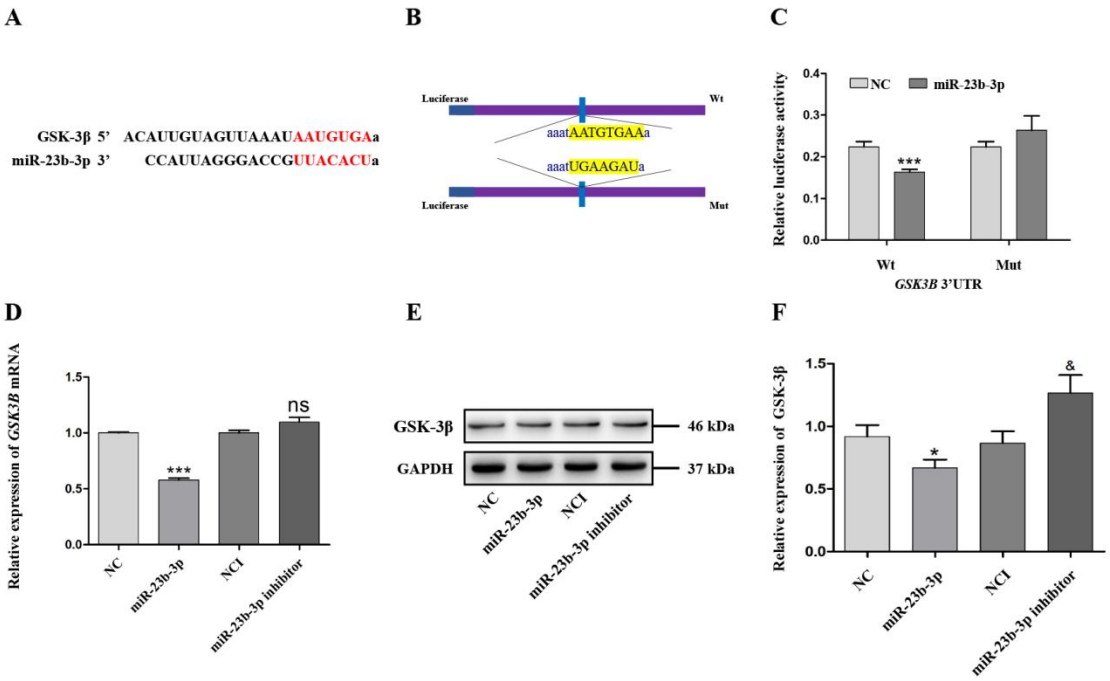

Additional Figure 5 miR-23b-3p negatively regulates GSK-3β.

(A) Computational identification of potential binding sites for miR-23b-3p in the 3'-UTR of GSK-3β. (B) Construction of the recombinant Luc-GSK-3β-Mut and Luc-GSK-3β-Wt. (C) Changes in relative luciferase activity in each group after transfection. miR-23b-3p mimics exerted a significant inhibition of reporter luciferase activity in the construct with Luc-GSK-3β-Wt, but not in the Luc-GSK-3β-Mut in HEK293 cells. (D) GSK-3β mRNA expression level after transfection of APPswe cells with miR-23b-3p mimics, miR-23b-3p inhibitor, or NC/NCI. (E, F) GSK-3β protein expression after transfection of APPswe cells with miR-23b-3p mimics, miR-23b-3p inhibitor, or NC/NCI measured by Western blot. GSK-3β protein expression in APPswe cells was significantly decreased after miR-23b-3p transfection compared to NC, but increased following miR-23b-3p inhibitor transfection compared to NCI. Data are presented as mean ± SEM, $n = 3$. $^{*}P < 0.05$, $^{***}P < 0.001$, *vs.* NC; $^{\&}P < 0.05$, *vs.* NCI. GAPDH: Glyceraldehyde-3-phosphate dehydrogenase; GSK-3β: glycogen synthase kinase 3beta; NC: negative control; NCI: negative control inhibitor; Wt: wild-type.

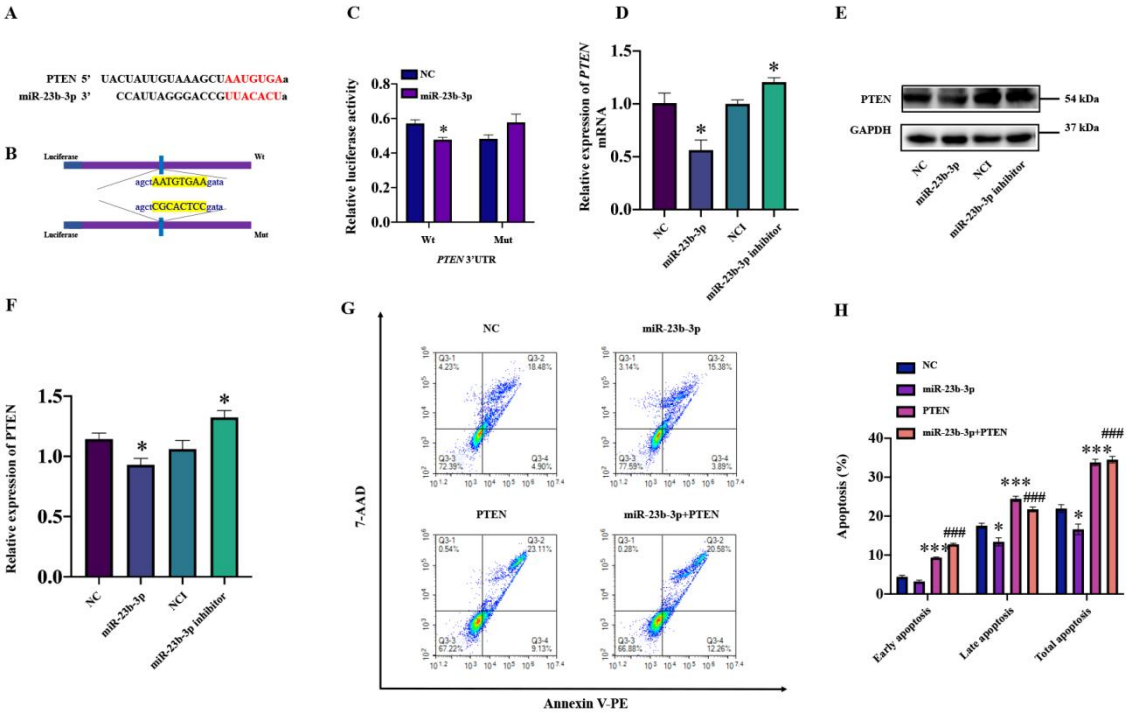

Additional Figure 6 miR-23b-3p negatively regulates PTEN.

(A) Computational identification of binding sites for miR-23b-3p in the 3'-UTR of PTEN. (B) Construction of the recombinant Luc-PTEN-Mut and Luc-PTEN-Wt. (C) Changes in relative luciferase activity in each group after transfection. miR-23b-3p mimics exerted a significant inhibition of reporter luciferase activity in the construct with Luc-PTEN-Wt, but not in the Luc-PTEN-Mut in HEK293 cells. (D) PTEN mRNA expression after transfection of APPswe cells with miR-23b-3p mimics, miR-23b-3p inhibitor, or NC/NCI. (E, F) PTEN protein expression after transfection of APPswe cells with miR-23b-3p mimics, miR-23b-3p inhibitor, or NC/NCI measured by western blot. PTEN protein expression in APPswe cells was significantly decreased after miR-23b-3p transfection compared to NC, but increased following miR-23b-3p inhibitor transfection compared to NCI. (G) Representative images indicating the effect of miR-23b-3p and PTEN overexpression on APPswe cell apoptosis induced by 300 μM copper assessed by flow cytometry. (H) Quantification of APPswe cell apoptosis caused by 300 μM copper in the presence of miR-23b-3p and PTEN overexpression. Data are presented as mean ± SEM, $n = 3$. $^{*}P < 0.05$, $^{***}P < 0.001$, *vs.* NC/NCI; $^{\#\#\#}P < 0.01$, *vs.* miR-23b-3p. GAPDH: Glyceraldehyde-3-phosphate dehydrogenase; NC: negative control; NCI: NC inhibitor; PTEN: phosphatase and tensin homologue deleted on chromosome 10; Wt: wild-type.

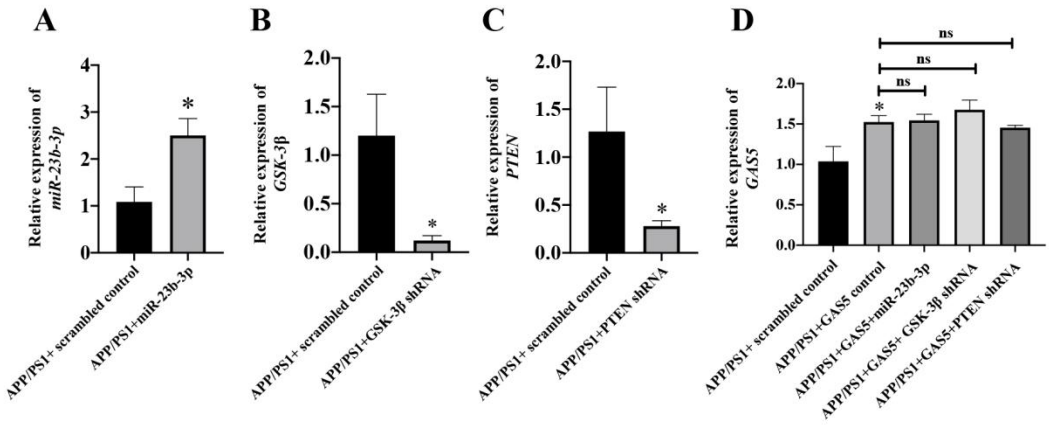

Additional Figure 7 Levels of miR-23b-3p, GSK-3β, PTEN, and GAS5 in different treatment groups for APP/PS1 mice. Increased miR-23b-3p levels (A), decreased levels of GSK-3β (B) and PTEN (C) in the hippocampus of APP/PS1 mice after intracerebroventricular injection of AAVs-scrambled sequences, AAVs-miR-23b-3p, AAVs-GSK-3β shRNA, and AVVs-PTEN shRNA, respectively. D Increased levels of GAS5 in the hippocampus of APP/PS1 mice after intracerebroventricular injection of AAVs-scrambled sequences, AAVs-GAS5, AAVs-GAS5+miR-23b-3p, AAVs-GAS5+GSK-3β shRNA, and AVVs-GAS5+PTEN shRNA. Data are presented as mean ± SEM, $n = 3$. $^{*}P < 0.05$, *vs.* APP/PS1+ scrambled control. AAVs: Adeno-associated virus; APP/PS1: APPswe/PSEN1dE9; GAS5: growth arrest-specific 5; GSK-3β: glycogen synthase kinase 3beta; PTEN: phosphatase and tensin homologue deleted on chromosome 10; Wt: wild-type.

Additional Table 1 List of aberrant lncRNA GAS5 expression from the cortex of 7-month-old 5×FAD mice and 9-month-old APP/PS1 mice using high-throughput sequencing analysis

	9-mon-old WT mice (7-mon-old WT mice)			9-mon-old APP/PS1 mice (7-mon-old 5×FAD mice)			*P*-value
	WT-1	WT-2	WT-3	APP/PS1-1 (5×FAD-1)	APP/PS1-2 (5×FAD-2)	APP/PS1-3 (5×FAD-3)	
GAS5 in APP/PS1mice	2.241349	2.251351	2.192762	2.421618	2.315439	2.34187	0.02
GAS5 in 5×FAD mice	1.33	1.69	1.42	2.46	1.93	2.14	0.02

-1, -2, -3: The sample size was 3 (n=3), and the numbers represented the levels of three mice, respectively. APP/PS1: APPswe/PSEN1dE9; GAS5: growth arrest-specific 5; WT: wild-type.

Additional Table 2 Analysis of the conservation of binding sites between growth arrest-specific 5 and four target genes

microRNA family	Seed position	Conservation		
		Primates	Mammals	Other vertebrates species
miR-23b-3p	chr1:173833704	56%	4%	0
miR-23b-3p	chr1:173835512	22%	0	0
miR-10a-5p	chr1:173833210	56%	0	0
miR-135a-5p	chr1:173835675	56%	0	0
miR-135a-5p	chr1:173835859	33%	0	0
miR-1297	chr1:173833308	56%	35%	0
miR-1297	chr1:173833329	44%	78%	0